PRODUCTION AND OPTICAL PROPERTIES OF GOLD NANO-CLUSTERS

CHENHAO LI

Submitted in fulfillment of the requirements for the Mphil's degree

Department of Physics

University of Strathclyde

2013

Declaration of Authenticity and Author's Rights

This thesis is the result of the author's original research. It has been composed by the author and has not been previously submitted for examination which has led to the award of a degree.

The copyright of this thesis belongs to the author under the terms of the United Kingdom Copyright Acts as qualified by University of Strathclyde Regulation 3.50. Due acknowledgement must always be made of the use of any material contained in, or derived from, this thesis.

Signed: Chenhao Li

Date: May 13th 2012

Abstract

This project investigated the optical properties of chemically synthesized gold nano-clusters (AuNCs) and creation of size selected AuNCs using physical method.

In the chemical method, bovine serum albumin (BSA) was used to stabilize AuNCs. BSA-Au_{25} was synthesized with an emission band observed at around 600~700nm. The dynamical study revealed a slow decay process with a fluorescent lifetime found to be as long as 1.2μs. Moreover, this work studied the size of BSA-Au_{25} through fluorescence anisotropy measurement. The investigation on the size at different pH values revealed a dramatic change in particle size as pH reduced to 3.1, consistent with the change of BSA from N form to E form. This study suggests the possibility of exploiting fluorescent protein-gold nano-clusters to probe protein conformational changes. To investigate the size dependent fluorescence behaviour, a size selected nano-cluster source has been employed to produce bare AuNCs. So far, Au_5 and Au_8 have been observed. In the future, the optical properties of the bare AuNCs will be compared with that of BSA-Au_{25} to understand the fluorescence mechanism of AuNCs.

Table of Contents

1. Introduction

1.1 Background

Gold is one of the most widely used noble metals for adornment because of its chemical stability, good ductility as well as its beautiful surface color. When the size of gold becomes as small as hundreds nanometers or even smaller, it shows unique properties which make gold much more interesting scientifically. Therefore scientists have investigated the properties, microstructures and applications of nano-gold with different sizes and different shapes[1].

Nano-scale gold is generally classified into three main categories [2, 3]: when the size of nano-scale gold is comparable to the length scale of visible light wavelength or $R \approx \lambda$ (R is the radius of gold particle which is supposed to be sphere, λ is the wavelength of visible light), such gold materials are classified as large gold nano-particles (AuNPs). The optical properties of large AuNPs match the properties of Mie scattering. When the sizes of nano-scale gold reduce to the sizes which are comparable to the length scale of electron mean free path or $R \leq \lambda$, the materials are classified as small AuNPs. The optical properties of small AuNPs such as surface plasmon resonance are size dependent, which are different from the properties of large AuNPs which are just correlated to the volumes and dielectric functions. When the sizes of nano-scale gold are comparable to Fermi wavelength of an electron or ~0.5nm for gold, they are classified as gold nano-clusters (it is abbreviated as AuNCs in this thesis). The optical properties of AuNCs are totally different from the former two categories. For example, the surface plasmon absorption exists in the absorption spectrum of both large and small AuNPs, while this phenomenon disappeared in the absorption spectrum of AuNCs. This difference is shown in figure 1.

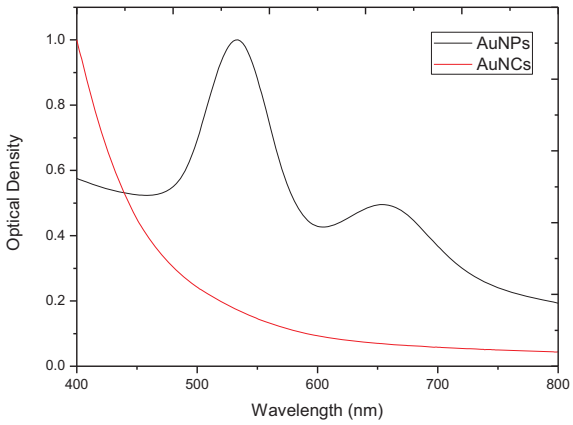

Figure 1 The comparison of absorption spectrum between AuNPs (size ~50nm) and AuNCs (size ~0.9nm). The absorption spectrum of AuNPs shown in this figure was obtained by courtesy of my colleague Yinan Zhang.

From figure 1, it can be seen that there is a double-peak (because of the particles' shape) in the absorption spectrum of AuNPs, but it is smooth in the absorption spectrum of AuNCs. It is clear that there is no surface plasmon resonance in AuNCs solution. This is because the AuNCs are too small to support the surface plasmon resonance.

The essential difference between AuNCs and other two types of AuNPs is that the former one exhibits the molecule-like behaviour such as discrete state due to the quantum confinement [4]. In Zheng's report, the discrete emission energy predicted by Jellium Model which is given as $E_f/N^{1/3}$ coincides with the experimental result well. In the formula, E_f represents Fermi energy level, and N represents the number of atoms exists in each AuNCs. It is suggested that there are two different possible explanations for the mechanism of the observed emission from AuNCs. One is related to the

intraband (sp/conduction band) transition and the other is correlated to the interband (d-sp) transition [3, 5]. AuNCs and their optical properties are investigated and discussed in this thesis.

In recent years, AuNCs have been paid more and more attention because of their great potential in chemical catalyst such as CO catalyst [6], metal ions sensors to detect Hg^{2+} or Cu^{2+} ions [7, 8], bioengineering labels to labeling the cancer cells [9], drug delivery in disease therapy [10] and so on. In this project, AuNCs were generated through chemical method as well as by physical method. The optical properties and some potential applications of AuNCs were investigated.

The rest of this chapter provides a survey on AuNCs regarding the generation, the microstructure, the optical properties as well as the recent applications on AuNCs. Chapter 2 shows the background knowledge for experimental methods adopted in this project. The experimental study on optical properties of AuNCs and their response to metal ions are discussed in Chapter 3. This thesis finishes with conclusions and future outlook presented in Chapter 4.

1.2 Production of AuNCs

Many methods have been developed to generate AuNCs in recent years. Typically, synthesized AuNC is formed by coating a gold core which contains several gold atoms with an outer structure. Au NC contains bare gold core can be obtained by physical yield method. Both chemical methods and physical methods were adopted in this project.

1.2.1 Chemical methods

Several methods of synthesizing AuNCs in solution have been developed in recent

years [2]. So far, AuNCs have been stabilized or synthesized mainly with Poly(amido)amine dendrimer (PAMAM), Tetrakis Hydroxymethyl Phosphonium Chloride (THPC), Bovine Serum Albumin (BSA), Deoxyribonucleic acid (DNA) and so on.

For visible emission PAMAM-AuNCs reported by Zheng [11], PAMAM dendrimer is utilized to encapsulate AuNCs to synthesize a high quantum yield fluorophore. The typical method to synthesize PAMAM-AuNCs is to dissolve 0.5 μmol G4-OH or G2-OH and 1.5 μmol $HAuCl_4 \cdot 5H_2O$ (Aldrich) into 2 mL of deionized water (18 MΩ), then slowly add an equivalent of $NaBH_4$ (0.005 M) into the solution within 30 mins to reduce the gold. Keep stirring the solution for two days until reaction and aggregation processes were completed, and then centrifuge (16,000 g) the sample for 1 hour to remove the large gold nanoparticles. A set of fluorophores can be acquired from changing the molar ratio between gold ions and dendrimer [3, 5, 12]. UV- emitting gold clusters can be created by adding 0.5 μmol G2-OH and 0.5 μmol $HAuCl_4$ into 2 mL distilled water. Green-emitting gold clusters were synthesized by adding 0.5 μmol G2-OH and 3 μmol HAuCl4 into 2 mL distilled water. Red and IR emitting gold clusters can be preferentially synthesized by adding 6.0 μmol and 7.5 μmol HAuCl4, respectively, into 2 mL water mixed with 0.5 μmol G4-OH or G4-NH_2.

For the purpose of synthesizing red emission AuNCs, a method to synthesize DPA-AuNCs was reported in Shang's work [13]. Mild reductant THPC was utilized in this method, and DPA was adopted to stabilize gold clusters. The procedure of production is as below: 47 ml NaOH solution (6 mM) was added into 12 ml THPC (80%) solution at 37 °C. The mixture was stirred for 3 mins, then $HAuCl_4$ (0.67 ml, 2% by mass) and DPA (2.5 ml, 0.1 M) were added rapidly into the former mixture. The solution was stirred for 15 hrs until the color turned to light yellow. Then, in the centrifuge progress, the as-prepared AuNCs was purified by Nanosep filters.

BSA-AuNCs were first reported by Xie who adopted a very simple method to synthesize AuNCs. It is described as below: aqueous $HAuCl_4$ solution (5 mL, 10 mM, 37 °C) was added to BSA solution (5 mL, 50 mg/mL, 37 °C) with strong and continuous stirring. Then, add NaOH solution (0.5mL, 1M) into the mixture 2 mins later. Keep shaking the solution at 37 °C for 12 hrs [14]. This method is very hard to optimize until Guével and his coworkers introduced a modified method based on Xie's approach. They mixed 5 mL aqueous solution of $HAuCl_4$ (10 mM) with 5 mL of bovine serum albumin (BSA 96%; 20 mg/mL) under vigorous stirring at 37 °C, then, added 50 mL of ascorbic acid (0.35 mg/mL), introduced 0.5 mL of NaOH solution (1 M) 5 mins later, kept the solution at 37 °C for 5 hrs. [15].

Besides the methods introduced above, some other groups have reported more approaches as introduced below:

Hui Wei reported in his paper that they synthesized their AuNCs in the following way: First, add 100 μL of 4 mM HAuCl4 and 100 μL of 10 mg/mL lysozyme aqueous into 100 μL water, then mix them together. Add 10 μL of 1 M NaOH 5 mins later, then mix them at 37 °C overnight [16].

Hussain reported a "one step" method to prepare the particles. They use a freshly prepared solution of sodium borohydride (2 mL, 50 mM) to reduce aqueous solution of hydrogen tetrachloroaurate (20 mL, 0.5 mM) in the presence of a water-soluble alkyl thioether end-functionalized poly (methacrylic acid) stabilizer. By changing the polymer concentration, they acquired a set of fluorephore [17].

Bao reported in his paper that they tried a set of good buffer to synthesize AuNCs. In their experiment, they mixed Au(III) chloride aqueous solution (5.8 mM, 1 mL) with a Good's buffer (100 mM pH 7, 5 mL) at room temperature, with subsequent incubated shaking for three days (37 °C, 250 rpm). In the process of metal cluster synthesis, gold nanoparticles are formed first, and only after many days are the

fluorescent clusters formed after the particles dissolved in the reaction medium [18].

1.2.2 Physical methods

There are several physical methods to generate AuNCs, such as the gas condensation method [19], laser vaporization method [20], sputtering-deposition methods [21, 22], high temperature matrix preparation techniques (HTMP) [23], and a so-called pick-up method [24]. In the gas condensation method, metal in the crucible is heated and evaporated. Then, the vapor is cooled down by being mixed with cold gas. The size of the clusters is controlled by supersonic inhibition. In this method, the generated clusters are neutral clusters, which mean they are difficult to accelerate in the subsequent process. In the laser vaporization method, the target metal is evaporated by pulsed laser, and cooled down to form clusters by pulsed cold inert gas flow. The advantage of this method is the available size range of clusters is very huge, but the problem is very apparent - the clusters are neutral which means it is not able to do size selection by electrical or magnetic field and it wastes a lot of power in this method. In the sputtering –deposition method, noble ions are sputtered by primary ions (eg. in this work, the primary ions are vaporized Cs^+ ions) on the surface of the target metal. The sputtered positive or negative ions are mass selected in the subsequent process, and then deposited on the sample substrate, in some experiments, together with rare gas to form a matrix formed neutral sample on the substrate. In this method, clusters' size is limited under 30 atoms because the clusters' density decreases sharply as the size of cluster goes up to 20~30 atoms. In the HTMP method, metal atoms are heated in a resistively heated Knudsen cell, evaporated into the container full of rare gas and then cooled down by the wall cooled by liquid Nitrogen, finally, landed on a quartz plate. In the last method, argon clusters are allowed to go across the metal atoms

to ‘pick up’ the metal clusters. The size of the metal clusters in this method is controlled by the size of argon clusters and density of initial metal atoms. The mass selection function can be integrated in the sputtering-deposition system which means the size of the cluster produced based on this method is more controllable. It is believed that this method is very suitable for the production of small clusters with selected sizes ranging up to 30 atoms [25].

In Liu’s report, AuNCs were synthesized by adding 100 μL 0.1 M aqueous $HAuCl_4$ into 10 mL of N, Ndimethylformamide. Then, the mixture was evaporated in a vacuum environment and mass selected through a mass selection device and then dried after it is roughly purified by centrifuge [26]. In this half physical-half chemical method, cluster size is accurately controlled. But the problem with this method is that the process is too complex compared with other pure chemical methods, and it wastes too much time compared to the pure physical method.

1.2.3 Comparison between chemical and physical methods

The physical method using size-selected cluster beam technique can generate nano-clusters with good control over sizes and clean surface, which provides a good model system for investigating the fluorescence mechanism and size-dependent optical properties. On the other hand, chemical synthesis allows low cost, mass production of NCs. In this work, I studied the production of AuNCs using both approaches. In terms of chemical synthesis, Xie’s method became our first choice because this method uses protein (bovine serum albumin) and nontoxic chemicals that are harmless to the environment. Moreover, it is a “one step” process while the other processes are more complicated. The AuNCs generated through this method have higher quantum yield (6%) than those prepared by other methods. Bovine serum

albumin is a good agency: it can be attached to the cells or be attached to some other bio-chemical material such as folic acid, antibody. That means there may be an application possibility in the bio-engineering field for BSA-AuNCs.

1.3 Microstructure of AuNCs

AuNCs with coating have the structure containing 3 parts: core, which is stacked by pure gold atoms; bonding layer, which combine core atoms with coating molecules; and coating. We take thiol protected AuNCs as the example to explain the microstructure of AuNCs as the microstructure of this type of AuNCs have been extensively investigated and reported by many groups.

It is very important to make the microstructure of the outer structure or the binding layer clear -including how the structure forms, what the structure contains and how it combines with inner structure or gold core, because this could be the reason why AuNCs show some special optical properties such as with long lifetime which will be discussed in the following sections. In a related field, Whetten studied thiol protected Au_{102} and characterized the structure of Au[I]-thiol complex shown in figure 2 left scheme [27]. Moreover, Jadzinsky investigated the microstructure of p-mercaptobenzoic acid (p-MBA)-protected Au_{102}. The Au-S bonding structures of thiol-protected Au_{102} (Au_{102}(p-MBA)$_{44}$) determined by X-rayin Jadzinsky's work is shown in figure 2 right scheme [28]. The typical boding model can be simply written into $[S–Au(I)]_n$. Both of these two structures are very similar to each other as both of them are formed by binding several Au-S cells together to form an endless circle or hex circle as shown in figure 2.

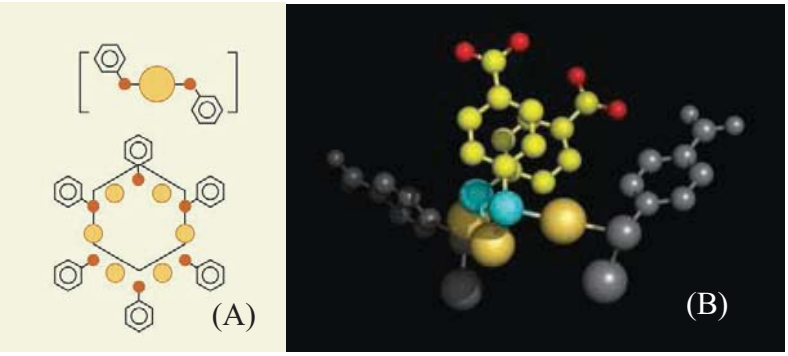

Figure 2 (A) The microstructure of Au-S bonding model in Au_{102}, yellow dots represent gold atoms, red dots represent sulfur atoms, the hexagons represent phenyl ($-C_6H_5$) aromatic hydrocarbon. (B) The microstructure of Au-S bonding model in $Au_{102}(p\text{-}MBA)_{44}$, the big yellow dots represent gold atoms, blue dots represent sulfur atoms, and the grey dots combine with yellow dots represent sulfur atoms in other cycles, the bigger grey dots represent gold atoms in other cycles. Other dots represent coating molecules. These two figures are from reference [27] and [28] respectively.

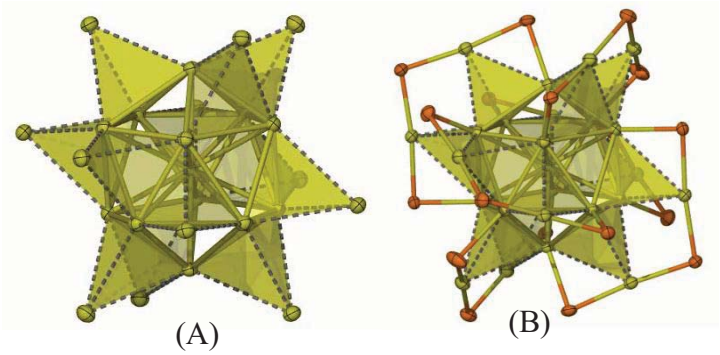

Figure 3 (A) The microstructure of gold core (dots connected by rod) together with the binding gold layer (dots connected by dash) in $[TOA^+][Au_{25}(SCH_2CH_2Ph)_{18}^-]$ which is determined by X-ray in Heaven's work. (B) The structural details about how binding Au atoms are combined with S atoms to form the binding layer. In both schemes, the yellow dots represent Au atoms, orange dots represent S atoms. Both of the figures are from reference [29]

As shown in figure 3, a much clearer microstructure of thiol protected AuNCs was

given by Heaven, it is assumed to be formed by a 13 atoms gold core coated with a layer containing 6 –[Au-S]$_2$– bonds through which the core is combined with the thiol contained coating. The microstructure model shown in figure 3 [29] was based on the result of X-ray measurement. In this model, a central Au atom and 12 surrounded Au atoms form the 13 atoms gold core, and other 12 Au atoms at outmost layer combined with S atoms form the binding layer. The atomic distance of gold atoms between the central one to the ones located on the shell of the 13atoms' core is 2.79±0.01 Å, the distance between other gold atoms in the 13atoms core is 2.93±0.06 Å. The Au-S distance from the combined gold core atom to adjacent sulfur atom is 2.38±0.01 Å, while the distance from the outermost gold atom to the adjacent sulfur atom is 2.32±0.01 Å. The atomic distance from outmost Au atoms to the adjacent ones on the shell of 13 atoms gold core is 3.16±0.07 Å. The global size of gold core together with the bonding atoms layer is confirmed to be 9.82±0.04 Å as shown in figure 4 (a) [29].

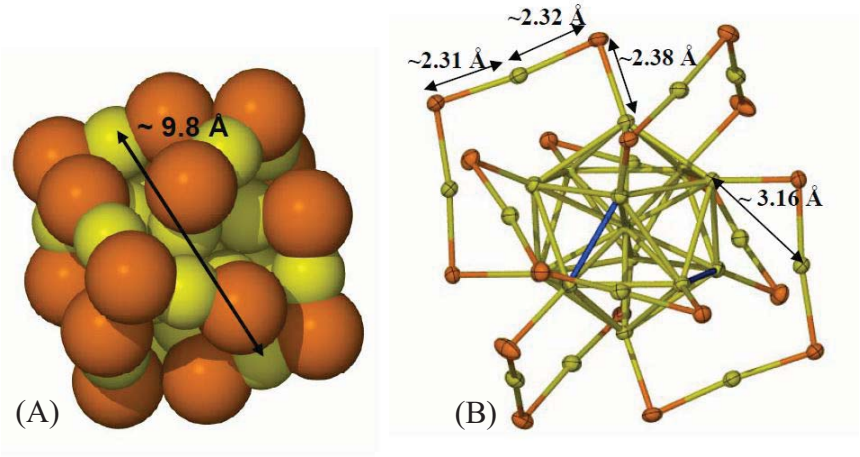

Figure 4 (A) The global size of gold core with binding atoms. (B) The atomic distances of Au-Au and Au-S, both of the figures are from reference [29]

In above figure, the Au-Au distance highlighted in blue is 2.79±0.01Å. The other Au-Au distances are 2.93±0.06 Å.

Based on Heaven's work, Simms has investigated the microstructure of BSA stabilized AuNCs [30]. It is confirmed by x-ray analysis that there are 6 –S–Au(I)–S–Au(I)–S– staple which surround the 13 atoms gold core. It is discussed in Simms's work that the Au-Au distance in the gold core is ~2.8 to ~2.9 Å which is coincident with the result given by Heaven. Furthermore, Simms has pointed out the Au-S bonds' distance which is 2.3 Å measured by X-ray measurement in his work is slightly shorter than the result 2.35 Å. This observation implies that the coating may affect the distance of the Au-S bonds.

It is expected that the microstructure of the protein coated AuNCs synthesized through reducing gold from $HAuCl_4$ by Bovine Serum Albumin (BSA) should have a similar structure as thiol-protected AuNCs. That is because there are 35 thiol groups in a single BSA molecule and some of them may form Au-S bonds [14]. XPS measurement confirmed the presence of Au(I) [14, 31], suggesting charge transfer from Au atoms to S atoms in the clusters [30].

1.4 Optical property of AuNCs

In recent years, optical properties of AuNCs have attracted intensive attention. AuNCs with varied emission bands ranging from blue to red have been synthesized through different processes and different coatings. This is reviewed in Lin's work [2]. As shown in figure 5, the emission of AuNCs is tunable by changing the gold core sizes and coating molecules. Especially, the synthesis method using PAMAM first reported by Zheng [12] allows control over the size of clusters by changing the ratio of gold ions to dendrimer.

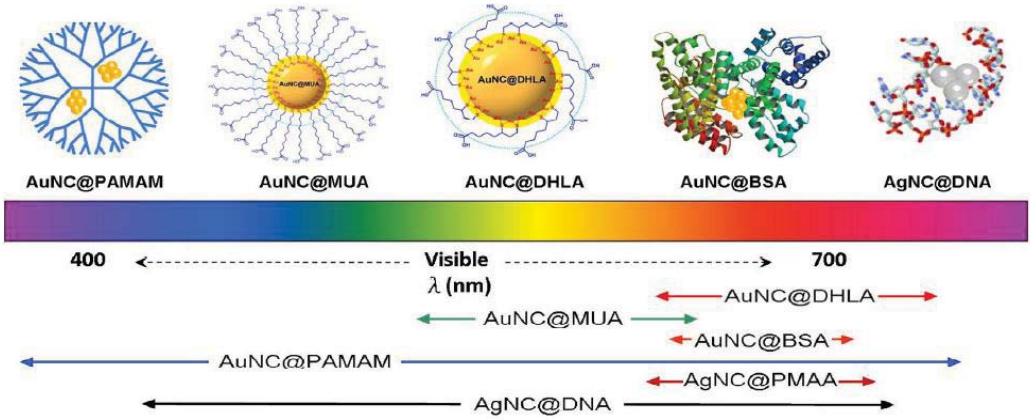

Figure 5 Different emissions of AuNCs with different coatings in the spectrum at the range from 400nm to 700nm. The figure is from reference [2]

Besides, Rath also reported a strong near UV (390~400nm) emission from their L-Cystein methyl ester hydrochloride stabilized Au_8 cluster [32]. Bao et al. tried a set of small polymers as stabilizing agency called "good buffer" to synthesize Au_{12} clusters with a excitation/emission of 395/500 nm in water [18]. Link et al. reported a $Au_{28}(SG)_{16}$ cluster which showed visible and infrared luminance [33]. Guével et al. reported the synthesis of AuNCs doped Si NPs which presented a bright reddish color under UV excitation [15].

The difference in optical properties against different functional ligands has been compared systematically by Liu et al [26]. In this work, bare Au_{11} was produced and then stabilized with different ligands. The optical properties of stabilized clusters are different with each other as shown in figure 6 when the coating molecule is changed. The emission intensity even raised by 5~6 times as the ligand molecules were changed from TA to DA.

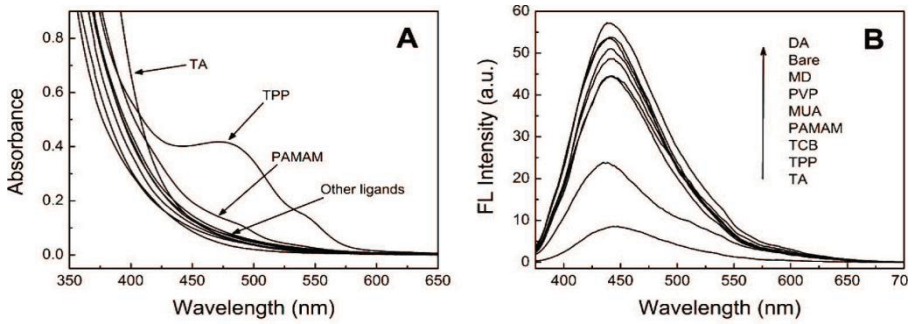

Figure 6 (A) The absorption spectra of Au_{11} with different coatings. (B) The emission spectra of Au_{11} with different coatings. Thioctic acid (TA), triphenyl phosphine (TPP), thiocholine bromide (TCB), poly(amido) amine dendrimer (PAMAM), 1-mercaptoundecanoic acid (MUA), polyvinylpyrrolidone (PVP), 1-dodecanethiol (DT), bare clusters (Bare), dodecylamine (DA). Both figures are from [26]

As early as 1985, Parmigani pointed that the optical properties of AuNCs are related to the synthesized process [34]. In recent years, the overall red shift in absorption with the increase of the gold core size is further discovered. Nijamudheen et al. concluded that, averagely one more Au-atom added to a Au_n cluster makes the spectra red-shifted by 15 nm [35]. Zheng's results as shown in figure 7 also support the conclusion that the emission red-shifts as the size of clusters increases [5].

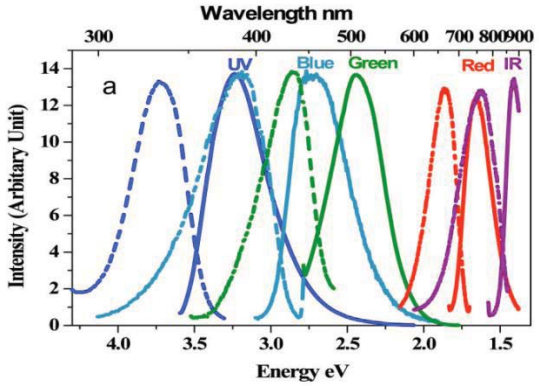

Figure 7 Excitation (dashed) and emission (solid) spectra of AuNCs with different size. The UV, blue, green, red and IR emission are from Au_5, Au_8, Au_{13}, Au_{23} and Au_{31} respectively. Figure is from reference [5]

For the purpose of potential applications in the future, high quantum yield clusters are required. A lot of method to synthesize high quantum yield AuNCs have been tried by researchers. For example, Zheng reported a blue emission Au_8 cluster [11] with a high quantum yield as high as 35%. This work is widely cited but argued by other researchers. Among gold clusters with sizes from Au_5~Au_{31} with corresponding emissions from ultraviolet to infrared, Au_5 is reported to have a quantum yield as high as 70% [12]. However, Duan reported a quantum yield of 10~20% from the Au_8 clusters synthesized by etching process [36]. Nicolas chose another method to synthesize a polymer coated AuNCs with a size up to 1.1 nm and obtained a quantum yield of 3% [37], and they believed the high quantum yield in Zheng's report may be caused by the dendrimer rather than Au core. Shang used a simple and different etching method and obtained the AuNCs with 1.3% quantum yield [13]. Lin et al. also synthesized a type of AuNCs capped with dihydrolipoic acid (DHLA) whose quantum yield is 1~3% [38].

1.5 Application of AuNCs:

The most important application of AuNCs is fluorescence labeling because of their extraordinarily optical properties, their ultra-small size (usually several nanometers or even smaller), non-toxicity, and highly fluorescent properties. Compared to semiconductor quantum dots, noble metal NCs are harmless to bio-cells. The preparation of AuNCs needs neither toxic precursor nor a complicated high temperature environment. Moreover, such sub-nanometer fluorescent metal clusters have well-defined excitation and emission spectra and can be used as an energy transfer pairs in biolabels.

It has been reported that AuNCs have the potential to serve as a Hg^{2+} detector [16].

Mercury is a pollutant which can be found in water and food sources, causing damages to the central nervous system, endocrine system and brain. In order to monitor or detect Hg^{2+}, lysozyme-stabilized gold fluorescent clusters (LsGFC) by mixing lysozyme and $HAuCl_4$ under basic conditions is proposed as a stable Hg^{2+} detector with high sensitivity and selectivity [16].

Gold clusters can also be used as an efficient catalyst in some chemical reactions. Lim et al. produced AuNCs as small as 20 atoms using evaporation with subsequently mass selection process [39]. It was reported that these NCs have an exceptional capability to catalyze a wide variety of chemical reactions, including the oxidation of poisonous carbon monoxide (CO) into harmless carbon dioxide at room temperatures. The results revealed that the most active AuNCs for CO conversion were bilayers of approximately 0.5~0.8 nanometer in diameter containing about 10 gold atoms [6].

In another example, gold cluster beam is used as secondary ionization as it gives a high spatial resolution and high ion yields [40]. The AuNCs system also can serve as a general purpose ion gun.

The aim of my research is to make gold clusters through both chemical and physical methods and to investigate their optical properties and potential application. In this report, some information regarding the gold clusters preparation and the preliminary results are documented.

2.Experimental Method

Two main methods were adopted to produce AuNCs in this thesis: wet chemical synthesis method and physical method adopting cluster source. Detailed information of the cluster production, the principle of the physical method will be presented in appendix 2 as the project producing gold clusters with physical method was in its very early stage,.

2.1 Chemical method to synthesize BSA-AuNCs

2.1.1 The synthesis of BSA-AuNCs

In this thesis, BSA-AuNCs were synthesized based on Xie's approach [14]. The stirring time was shortened to promote a faster preparation process.

In the typical experiment, aqueous HAuCl4 solution (5 mL, 10 mM, 37 °C) was added into BSA solution (5 mL, 50 mg/mL, 37 °C) with strong and continuously stirring. Two minutes later, NaOH solution (0.5 mL, 1 M) was added into the solution. The purpose of this step is to change the pH value to >12, it is one of the key point for the successful synthesis. Then, the solution was strongly stirred at 37 °C for ~6 hrs [14]. When this process was finished, the sample was incubated in a temperature controlling oven at 37 °C. The color of the solution changed to dark orange 24hrs later, which means the BSA-AuNCs were synthesized.

Reference sample was synthesized by adding HCl solution (50 μL, 1 M, 37 °C) into BSA solution (5 mL, 50 mg/mL, 37 °C) with strong and continuously stirring. The rest of the operation was totally the same as the preparation of gold clusters that was mentioned previously.

2.1.2 The principle of synthesis

The process of the wet chemical synthesis was described in Xie's work [14] which is shown in figure 8. In the synthesis process, Au(III) ions were trapped by the BSA protein molecules, then BSA reduce the trapped gold atoms when the environment pH is changed to ~12. Reduction progress occurred in situ to form BSA-AuNCs. It is reported in Xie's paper that the quantity of atoms stabilized in each cluster is 25 based on the experiment's result of Matrix-assisted laser desorption ionization time-of-flight mass spectrometry (MALDI-TOF) mass spectra. But it is believed that the quantity of atoms stabilized in each cluster is actually a typical Gaussian distribution if there is no purifying process before the measurement, with a maximum around 22~25 atoms. This point has been confirmed by MALDI-TOF MS measurement carried out by Guével [31]. In the subsequent sections, the samples synthesized in our project will be named BSA-Au_{25}.

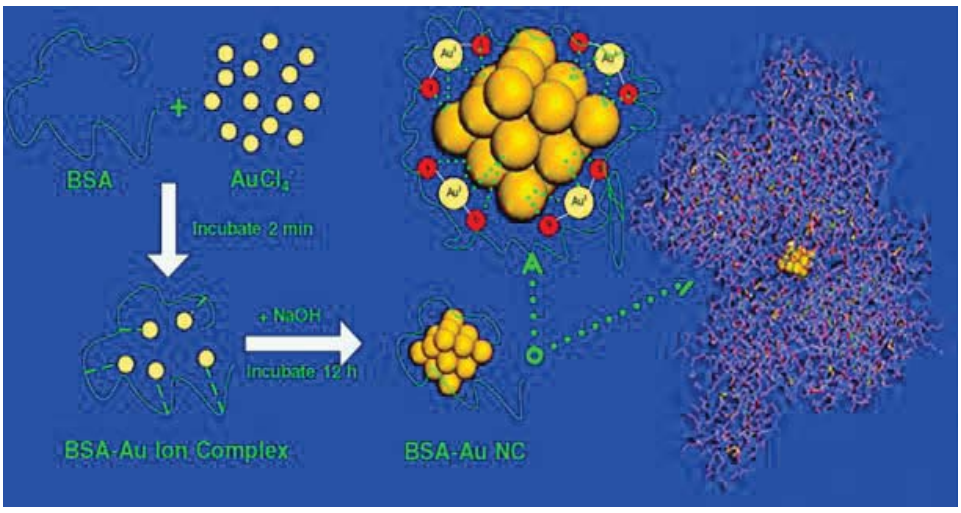

Figure 8 The scheme indicates the synthesis process of BSA-Au_{25} and the mechanism of synthesis process. Rough structure of BSA-Au_{25} is also given. Figure is from reference [14].

Moreover, Xie reported the existence of Au(I) ions in the BSA-Au_{25} which combine both gold core and the BSA coatings in a type of shell shape bonds. This oxidation state was determined by X-ray photoelectron spectroscopy (XPS). Also, it is confirmed that the ratio of Au(I) is around 17% [14]. The presence of oxidized gold atoms on the surface of gold core may be the key to explain the existence of long lifetime component of BSA-Au_{25}. This will be discussed in latter sections.

2.2 Characterization methods

2.2.1 Absorption Spectrum

The absorption spectra measurement is based on Beer-Lambert law as shown in figure 9.

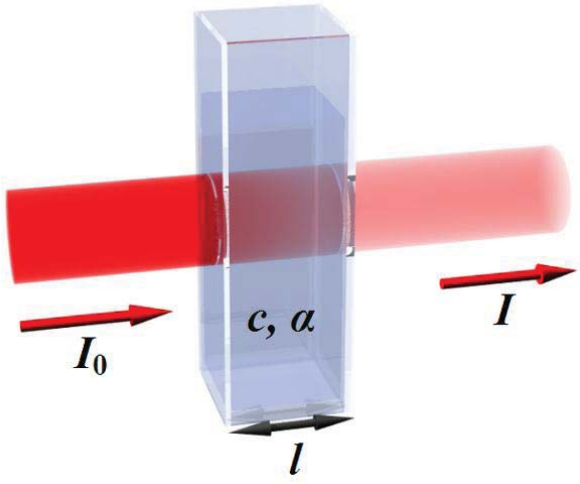

Figure 9 Absorption process occurred when the light go through solution in the cuvette. Figure from Wiki webpage (http://en.wikipedia.org/wiki/File:Beer_lambert.png)

The light transmission can be calculated following the equation bellow

$$T = \frac{I}{I_0} = 10^{-al} = 10^{-\varepsilon lc} \tag{1}$$

Where T represents the transmission of light which goes through the measured substance; I_0 and I represent the incident and transmitted light intensity respectively; l is the distance the light travels through the material; a is the absorption coefficient of the substance, ε is the extinction coefficient and c is the concentration of absorbing species.

Absorbance (A)/Optical density (OD) should be calculated out following the equation below:

$$A = OD = -\lg(\frac{I}{I_0}) = \lg(\frac{1}{T}) = al = \varepsilon lc \tag{2}$$

All the absorption spectra measurement in this thesis is carried out on the Spectrophotometer V660.

2.2.2 Fluorescence spectrum

The fluorescence process can be described by Jablonski diagram shown in figure 10. The fluorophore absorbs a photon and excited from ground state to excited state. When it goes back from excited state to ground state, it emits a photon. This process is called fluorescence process [41].

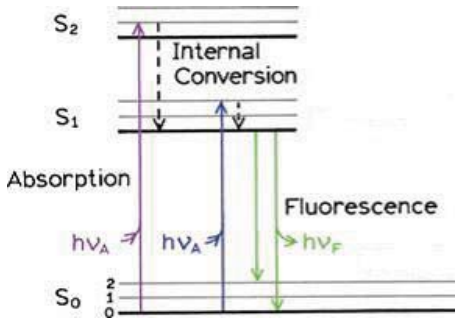

Figure 10 Jablonski diagram indicates the fluorescence process as well as the phosphorescence process. Graph is from reference [41]

The fluorescent emission intensity of a sample is usually measured by the spectrofluorometer described in figure 11. A commercial Fluorolog 3 spectrometer offered by HORIBA was adopted in this project.

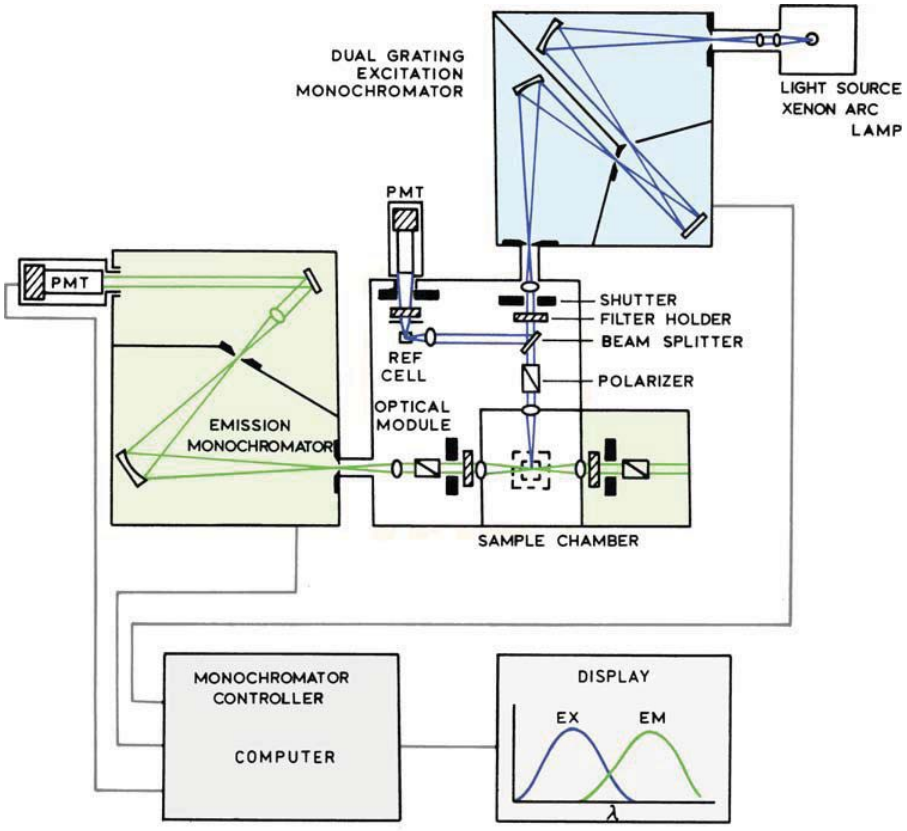

Figure 11 The sketch indicate the structure of spectro-fluorometer. Figure is from reference [41]

There is a 90° angle between the incident light route and the emission light route which is used to avoid interference from incident light. In the measurement process, incident light emitted by Xenon Arc lamp goes through the monochromator in which selected incident light is pointed the required wavelength. The shutter/slit is adopted to limit the width of transmission light's wavelength. A polarizer is utilized to offer a polarized light. On emission side, the equipment set up is almost the same as in the excitation light side. The only difference is the position there is a lamp installed a detector. The intensity of excitation light and emission light which is sensed by the detector will be pass to the computer and shown or calculated out automatically. In our experiment, a commercial spectra fluorometer Fluorolog was adopted.

2.2.3 TCSPC Technology

The fluorescence lifetime is defined as the average time fluorophore stays in the excited state. The fluorescence intensity can be simply described by exponential function as shown in equation 3

$$I(t) = I_0 e^{-t/\tau} \tag{3}$$

Where I_0 is the initial fluorescence intensity at the time t=0, τ represents the fluorescence lifetime. Normally, it contains several exponential components in the same system. For BSA-Au_{25} in this thesis, 4 exponential components were used to fit the lifetime decay curve of the sample to our knowledge.

Time-correlated single-photon counting (TCSPC) technology is the most widely used method to measure the lifetime. The principle of TCSPC is described in figure 12. A lot of channels are used to count the time a single photon is detected from when it is

excited in every recording round. Counts are accumulated in every channel. The intensity of photon distribution will be obtained in this case. When enough photons are collected by those channels, a decay curve can be developed by adding all the counts together.

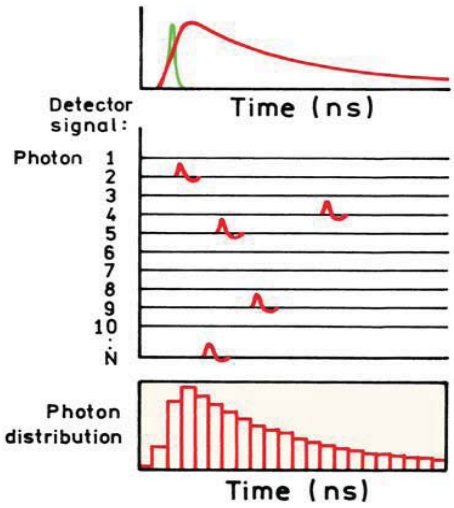

Figure 12 The scheme indicates the principle to form the lifetime decay curve, N channels are used to record the lifetime of every single photon in every round and the counts of every channel are accumulated to form the intensity of photon distribution, then the decay curve is formed. Figure is from reference [41]

The theoretical scheme of equipment is shown in figure 13

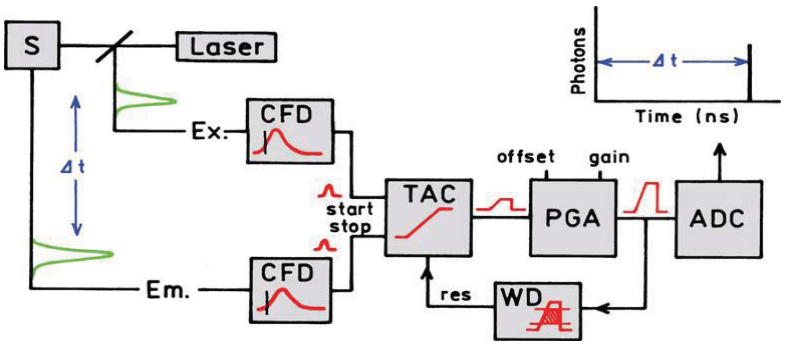

Figure 13 The scheme indicates the electronic structure of TCSPC equipment. It also illustrate how the device works. Figure is from reference [41]

The structure of lifetime measurement equipment is described following figure 13. Sample is excited by the laser from laser source. The time difference between when the time laser pulse is emitted and the time emission photon is detected should is considered as the fluorescence lifetime of the fluorophore. T_{ex} and T_{em} are received by constant fraction discriminators (CFD) and then the signals are passed to the time to amplitude converter (TAC). Then, as it is needed, the difference of voltage signal from T_{ex} and T_{em} respectively will be amplified by a programmable gain amplifier (PGA). Then the signal was converted to a numerical signal by the analog-to-digital converter (ADC). Additionally, the window discriminator (WD) is used to minimize the false readings by restrict the signal to given range of voltages. This process will be repeated to form a histogram of the decay.

The equipment we use to do the lifetime measurement of BSA-Au_{25} is FluoroCube offered by HORIBA, the structure of the kit is as shown in figure 14.

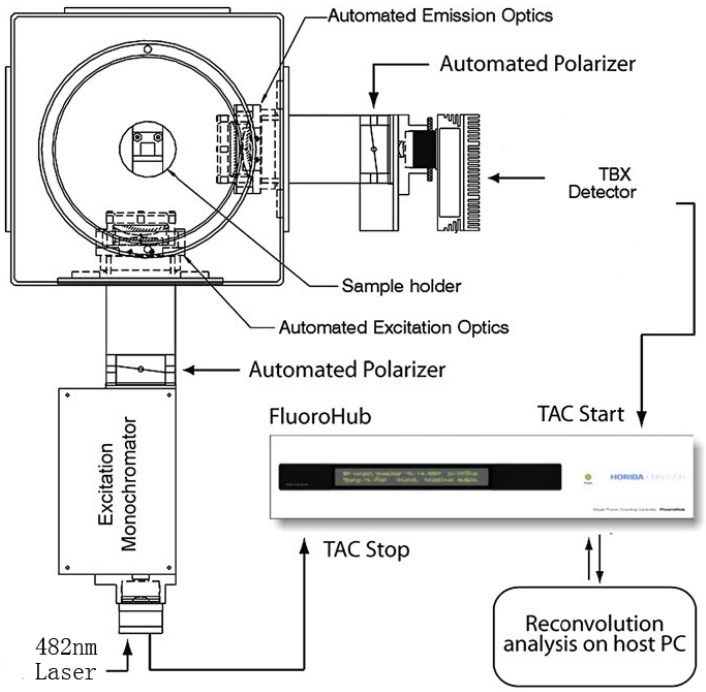

Figure 14 The graph shows the sketchy structure of lifetime measurement meter

The detected part of the emission spectrum was selected by use of a long pass filter (LP530) in front of the detector opposed to use of the monochromator. LP530 allows light with wavelength longer than 530 nm pass through to the detector while restricting light of any shorter wavelength.

2.2.4 Fluorescence Anisotropy Measurement

The fluorescence anisotropy measurement was also carried out on the HORIBA FluoroCube (figure 14). The experimental principle is as shown in figure 15 below.

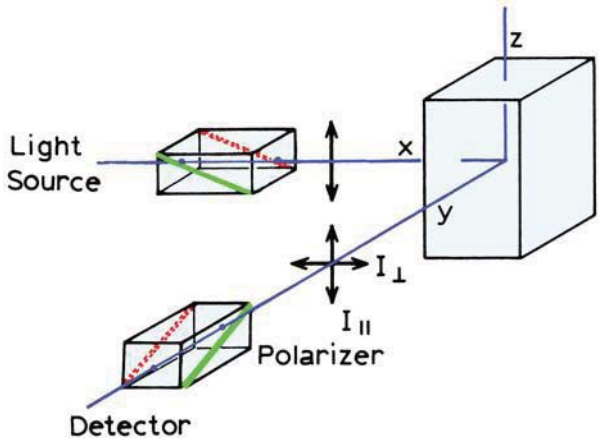

Figure 15 The scheme indicates the principle of fluorescence anisotropies' measurement. Figure is from reference [41]

The difference comparing the anisotropy measurement with the previously introduced TCSPC lifetime measurement is the employment of excitation and emission polarizer. When the two polarizers are oriented parallel to each other, the intensity observed is represented by $I_{//}$, while when the two polarizers are oriented perpendicular to each other the intensity observed is represented by $I_{\perp}$. The total

intensity is represented by I_T. The fluorescence anisotropy is calculated following the equation below:

$$r = \frac{I_{\parallel} - I_{\perp}}{I_T} = \frac{I_{\parallel} - I_{\perp}}{I_{\parallel} + 2I_{\perp}} \tag{4}$$

It can be derived from above equation that the anisotropy "*r*" is independent of the total intensity of the fluorescence, which means no matter how many counts are recorded in the same experiment the calculated fluorescence anisotropy should be the same. But, in actual experiment, more counts are beneficial otherwise the noise may be too big to be accepted.

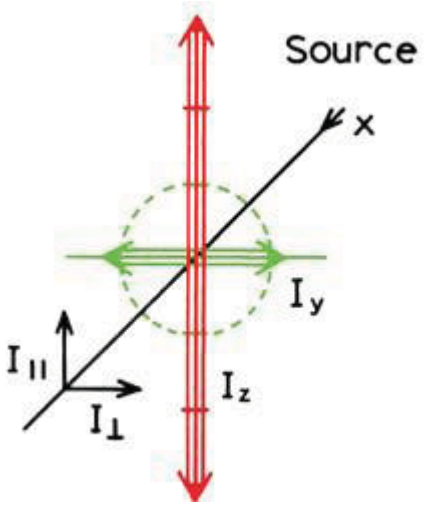

Figure 16 Polarization of a ray of light, [41]

Considering a vertically polarized system as shown in Figure 16 the fluorescence intensities are $I_z = I_{/\!/}$ and $I_y = I_{\perp}$, where I_x, I_y and I_z represent emission intensity along the x, y and z axis respectively. The total intensity is $I_T = I_x + I_y + I_z$ for any fluorophore. Each intensity is given by the square of the moment of transition projection on each axis so that the sum of three projections is unity. Suppose that the sample has z-axis symmetry, therefor, $I_z = I_{/\!/} + 2I_{\perp}$ [41].

3.Results and Discussion

3.1 Optical property of chemical prepared samples

3.1.1 Fluorescence of BSA-Au_{25}

Figure 17 shows the BSA reference sample (a) and chemical synthesized BSA-Au_{25} (b and c) under visible and ultraviolet light excitation respectively.

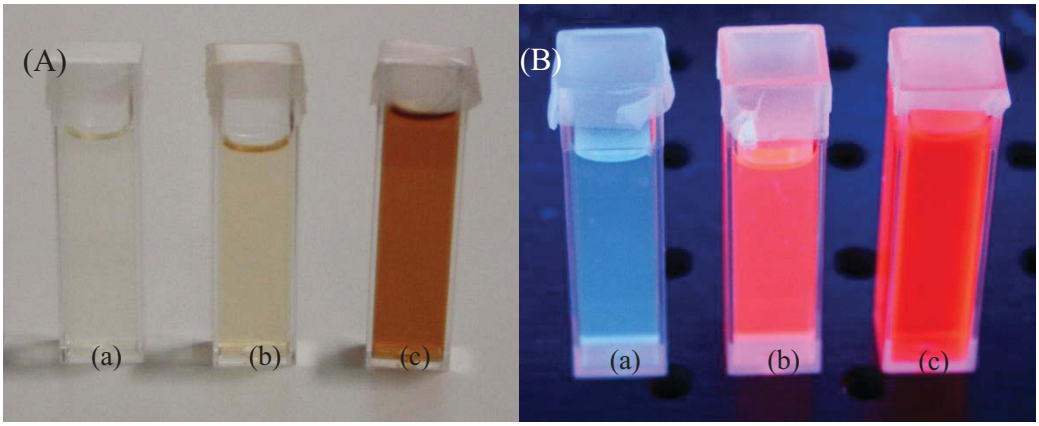

Figure 17 (A) Samples under visible light. (B) Samples under ultraviolet light excitation. The samples in each graph are (a) Reference sample, (b) BSA-Au_{25} diluted by 10 times, (c) BSA-Au_{25} original sample respectively.

It is found that all the samples in figure 17 are fluorescent under UV illumination. BSA reference sample emits blue light while both the BSA-Au_{25} samples emit red light. The difference in the emission wavelength indicates that the fluorescence of BSA-Au_{25} is arising from gold cores or at least related to the gold cores rather than from the BSA.

3.1.2 Absorption and Emission spectrum of BSA-Au_{25}

The same synthesis procedure has been repeated three times to confirm the reproducibility of this method. Absorption spectra and emission spectra of three resulting BSA-Au_{25} are shown in figure 18.

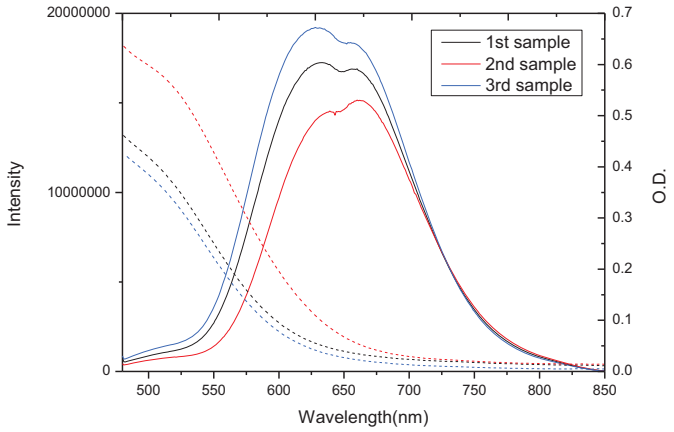

Figure 18 Absorption and emission spectra of three BSA-Au_{25} samples synthesized with the same procedure. The excitation wavelength is 470 nm.

The shapes of the absorption and emission bands of the all three samples are very similar. It shows the repeatability of this synthesis method. The slight change in the emission band may be caused by the slight difference in the experimental conditions including pH value, evaporation speed, reaction temperature and time.

It is apparent that there is no surface plasmon induced absorption band at the wavelength of 500~600 nm which is normally observed from the AuNP(s) samples. It suggests that the gold cores in BSA-Au_{25} are very small, not big enough to support surface plasmon resonance.

Considering the emission spectra, the emission band is broad and located at the wavelength from 600 nm to 700 nm. Two peaks at about 625 nm and 675 nm are visible, suggesting that there may be two bands overlapped in the emission band. It may arise from different gold core sizes as suggested by Guével that BSA-Au_{25} sample contains gold cores with different sizes ranging between 22~25 atoms [31]. Gold clusters of different structures may also give rise different emissions.

To further distinguish the fluorescence emission between BSA-Au_{25} and BSA, emission spectra of BSA-Au_{25} and reference sample is compared as shown in figure 19. The red line represents the fluorescence emission of BSA-Au_{25} sample, while the blue line represents the fluorescence emission of reference sample. It is clear that the reference sample has an emission band located at 500~550 nm, below the emission of BSA-Au_{25} when they are both excited at 470 nm. It should be noted that the emission band of BSA varies with excitation, as will be discussed in later section. This result confirms that the red emission is from BSA-Au_{25}, consistent with the observation discussed in previous section.

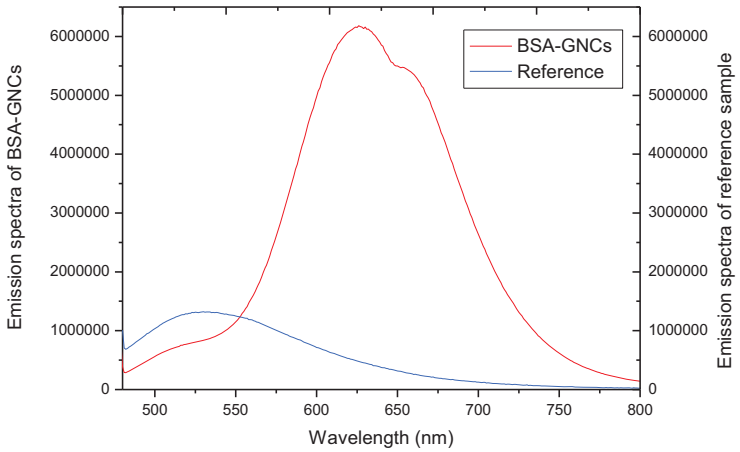

Figure 19 Comparison of emission spectra of BSA-Au_{25} and reference sample, excited 470 nm

To find out the best excitation wavelength for the BSA-Au_{25} sample the excitation spectrum of BSA-Au_{25} is measured and the result is shown in figure 20.

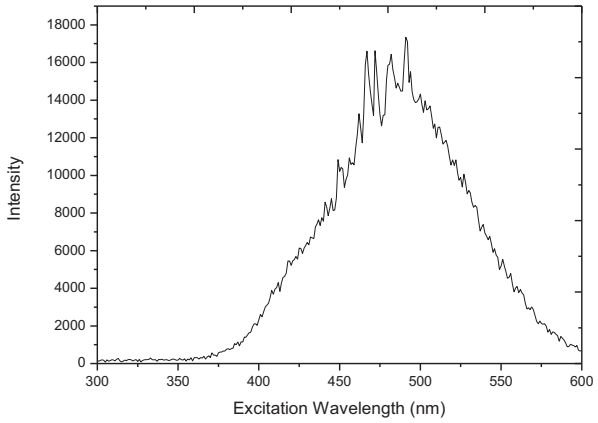

Figure 20 Excitation Spectrum of BSA-Au_{25} and Reference sample (emission set to 650 nm)

A peak located at around 470~510 nm is observed. In the subsequent experiment, the excitation wavelength between 470~485 nm was adopted. The emission spectra of BSA-Au_{25} excited at different wavelength are measured and shown in figure 21. Emission spectra of reference sample are shown in figure 22.

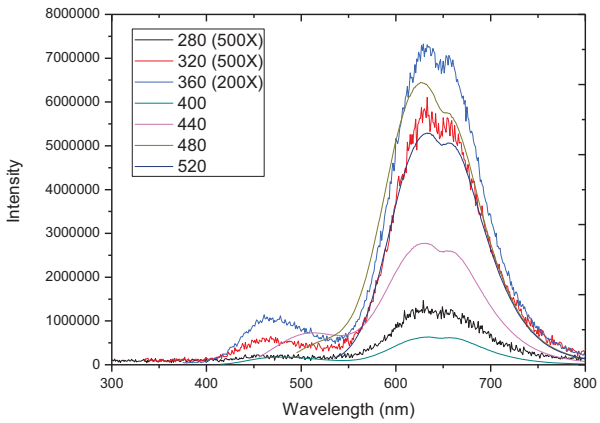

Figure 21 Emission spectra of BSA-Au_{25} at different excitation wavelength. Intensities of bands at 280nm, 320nm, 360nm were 500, 500, 200 times amplified respectively.

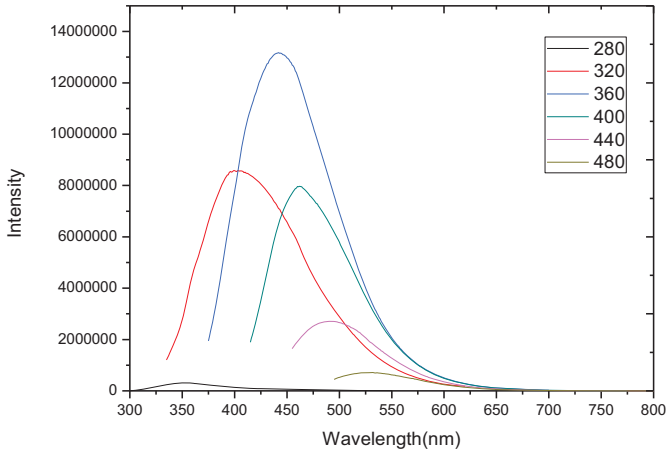

Figure 22 Emission spectra of reference sample at different excitation wavelength

Comparing these two graphs, two main points can be made. Firstly, the position of the red emission band, only found from BSA-Au_{25}, doesn't change as the excitation wavelength changes, but its intensity does. As the excitation wavelength increases from 320 nm to 520 nm, the intensity increases at first, then decreases. The fluorescence intensity peaks at around 480 nm, consistent with the excitation spectrum. Secondly, the position of emission at around 500~550 nm shifts to shorter wavelength as the excitation wavelength decreases from 480 nm to 280 nm. Its intensity also changes and peaks at around 360 nm. This trend is visible in figure 21, although it is more obvious from BSA reference sample as shown in figure 22. These observations confirm that the weak short wavelength emission found from BSA-Au_{25} sample arises from BSA, while the strong red emission is from BSA-Au_{25}.

3.1.3 Experimental effects on fluorescence of BSA-Au_{25}

For the purpose of investigating the experimental effect on the fluorescence of

BSA-Au_{25}, a series of experiments were carried out to study the influence of time, concentration and pH value.

For the purpose to confirm the stability of BSA-Au_{25}, a few samples were stored in sealed bottles in room temperature for five months. The emission spectrum has the same feature and a slight increased intensity compared with that taken five months before, as shown in figure 23 to confirm the stability of BSA-Au_{25}.

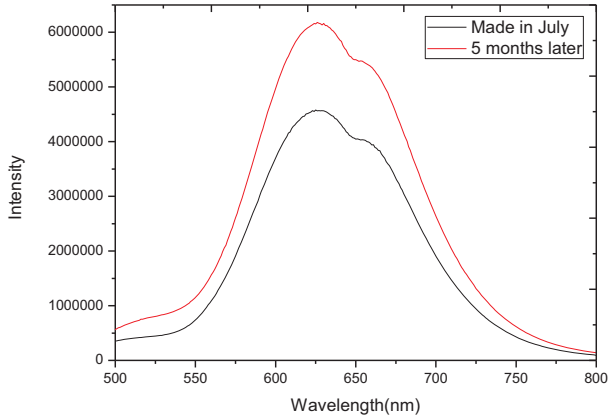

Figure 23 Difference of BSA-Au_{25}' emission bands between fresh sample and 5monthes stored sample

As made BSA-Au_{25} sample has a gold concentration about 5 mM and a high optical density far beyond 1.0. This high concentrated sample may affect the fluorescence behavior. So, the as made sample has been diluted. Figure 24 and figure 25 show the absorption and emission spectra of different diluted samples.

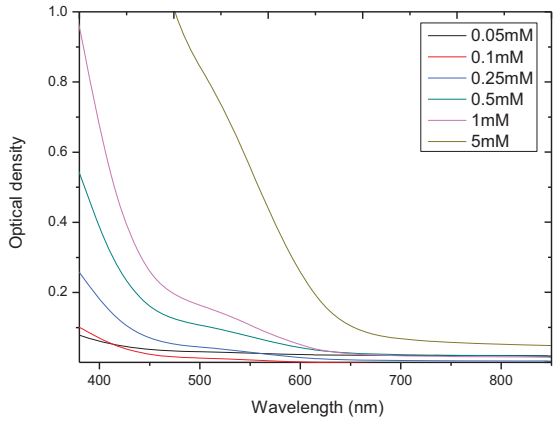

Figure 24 Absorption spectra of BSA-Au_{25} at different concentration

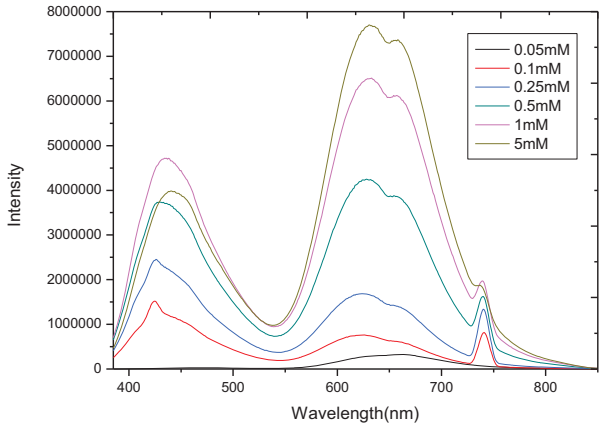

Figure 25 Emission spectra of BSA-Au_{25} at different concentration

As expected, the optical density and emission intensity of BSA-Au_{25} are closely related to the concentration of the sample. The relationship of emission intensity against [Au] concentration is however nonlinear as shown in figure 26.

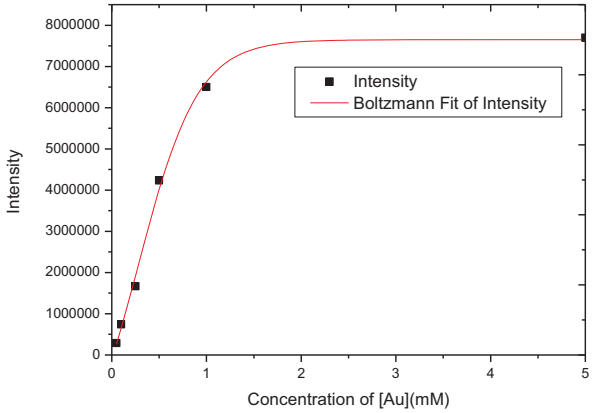

Figure 26 The emission intensity at peak point (625nm) against different concentration of [Au]

The fitted equation is as below:

$$I = 7648480 - \frac{11016650}{(1+e^{\frac{(C-0.275537)}{0.31733}})} \tag{5}$$

In this equation, *I* represents the emission intensity, C represents concentration of [Au]. The R-square is 0.9928.

At low concentration, the emission intensity goes up as the concentration of [Au] goes up, and the relationship between them is nearly a linear relationship. A near linear relationship can be seen from the samples with 0.05, 0.1, 0.25, 0.5 and 1 mM [Au], as shown figure 27. The relationship of emission intensity and concentration of [Au] can be represented as in equation below:

$$I = 152152 + 665090C, \tag{6}$$

where I represents the intensity, C represents concentration of [Au]. The R-square is 0.96459.

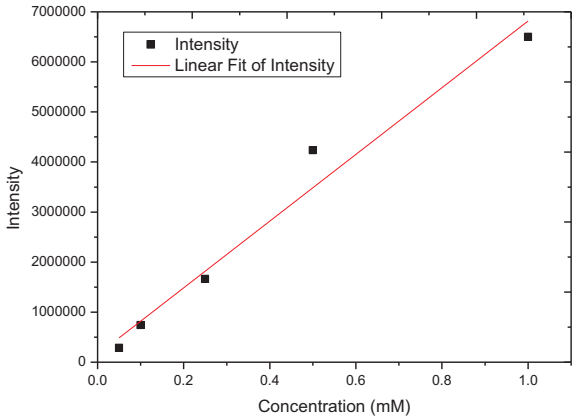

Figure 27 The linear fitting of the peak intensity against [Au] concentration for the former 5 points

But as the [Au] concentration goes too high to reach the value about 5 mM, the high optical density results in self-absorption and scattering that reduces emission. Therefore, a 20 times (20×) diluted sample with [Au] concentration of 0.25 mM is considered to be suitable for fluorescence study. Its optical density is not too high (<0.2) while the emission intensity is high enough. The following experiments in next section use sample at this concentration.

The last, but the most interesting part which will be discussed in this section is the influence of pH value on the fluorescence. In this experiment, HCl was induced into the sample to change the pH value of the as made sample. The final concentration of [Au] in each sample is ensured to be 0.25 mM by adding 0.2 ml original sample in which the [Au] concentration is 5 mM into 3.8 ml mixtures which contain 0.12 ml, 0.1 ml, 0.08 ml, 0.05 ml, 0.025 ml, 0 ml HCl with a concentration of 1 M respectively. The pH value was measured with the portable pH meter. Experiment results are shown in figure 28.

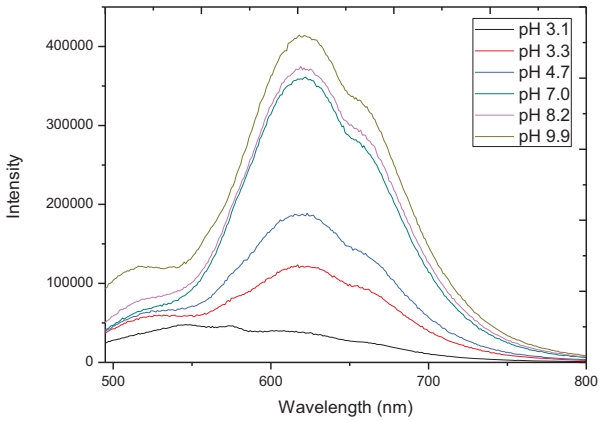

Figure 28 Emission spectra of BSA-Au_{25} at different pH value

It can be seen from figure 28 that the intensity of fluorescence falls down as the pH value goes down. Considering the unfolding of BSA at acidic environment (detailed in section 3.1.5), especially below pH 3.1, the decrease in emission implies that the fluorescence of BSA-Au_{25} is modified by the changing in the microstructure of BSA.

3.1.4 Fluorescence lifetime of BSA-Au_{25}

As mentioned in the previous sections, early work on the BSA-Au_{25} found a long fluorescence lifetime. It was assumed that this is due to the presence of gold core. In order to prove the concept that this slow decay process is the characteristic of fluorescence from BSA-Au_{25} rather than from BSA, a dynamical fluorescence study has been carried out in this work to compare the fluorescence decay processes from BSA-Au_{25} and the pure BSA that has the same concentration as in the BSA-Au_{25} sample.

Figure 29 displays the fluorescence decay curves of BSA-Au_{25}, BSA with NaOH as

in BSA-Au_{25} and pure BSA. It is clear that only BSA-Au_{25} has a significant slow decay process. Thus the long lifetime component is caused by gold core but not by BSA.

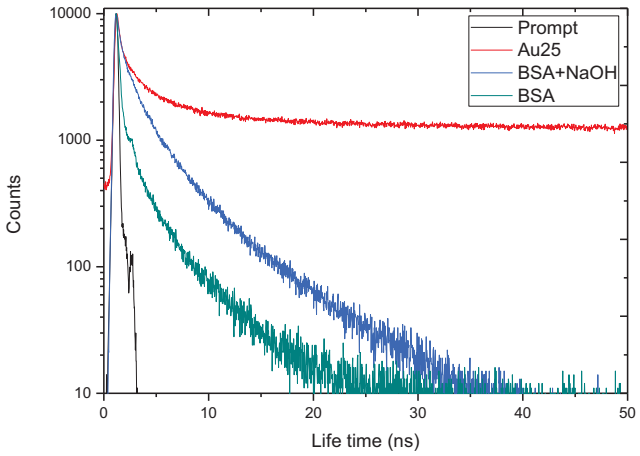

Figure 29 Comparison of lifetime decay curve between gold cluster sample and reference sample

The fluorescence mechanism and the source of the long lifetime is however not clear yet. Two mechanisms have been proposed to explain this slow decay process [31]. The first one suggests that this long decay lifetime is due to triplet-singlet intersystem transition. The other hypothesis considers the existence of oxidation states of gold atoms on the surface of gold core and suggests that the long lifetime component is caused by the oxidation state. This hypothesis is strongly supported by Guével's work. He found that there is no long lifetime component in the fluorescence process of BSA-Au_8 which does not have an oxidation state. In the later assumption, the long lifetime component is caused by the interaction between Au(I) and thiol, or between Au atoms. Wu found that the long lifetime fluorescence only exists when there are electron rich ligands on the surface of the gold clusters. Moreover, when replacing the ligands of Au_{25} clusters with electron rich ligands such as ligands containing [N] or

[O], the fluorescence of gold clusters is extremely enhanced [4]. This suggests the significant influence of gold–molecule interaction and the interface states on the fluorescence process. More work need to be done to fully reveal the fluorescence mechanism.

To fit the decay curve of BSA-Au_{25}, the fitting work is carried out by two steps: firstly, 2 μs rang was set to take the lifetime measurement and the long exponential decay part was fitted to obtain the value of the long lifetime component. The lifetime T= 1.2~1.3μs was obtained from the first step fitting results. Secondly, 50 ns TAC range was set for the measurement on the same sample and the short exponential decay was fitted, where one of estimating lifetime values was fixed to be the previous fitting result. The results show that the whole decay process is dominated by a slow decay process, with a lifetime in the micro-second scale, mixed with short decay processes with short lifetimes ranging from sub-nanosecond to several tens of nanoseconds.

The decay curves obtained in the two-step measurement separately are shown in figure 30. Subfigure (A) indicates the trend of the long lifetime component. In subfigure (B), the short component is shown more clearly. In the first step, the long lifetime decay was fitted by fitting the decay curve in the chosen fitting range as shown in figure 30 (A). One-exponential had been adopted to fit this long lifetime decay curve. Lifetime T was figured out in this step. Then, in the second step, four-exponential was adopted to fit the whole decay with one of lifetime values was fixed by the one obtained from the first fitting step. The number of exponentials was chosen to be 4 by considering the goodness of χ^2. The first stage one-exponential lifetime decay is described as:

$$I(t) = A + B_1 e^{-t/T1} \tag{7}$$

The second step four-exponential lifetime decay is described as:

$$I(t) = A + B_1 e^{-t/T1} + B_2 e^{-t/T2} + B_3 e^{-t/T3} + B_4 e^{-t/T4} \quad (8)$$

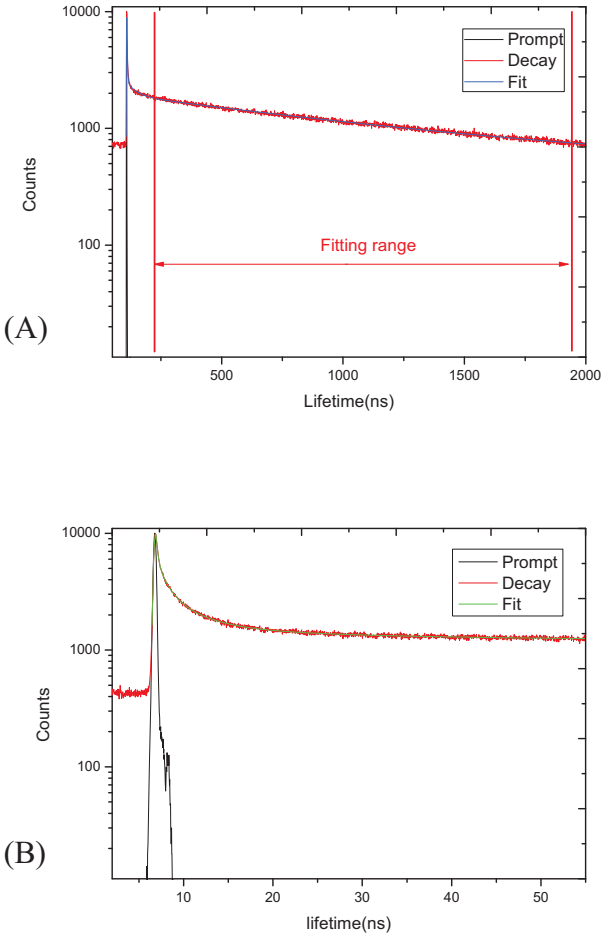

Figure 30 (A) The result is obtained with 500 KHz laser 2μs TAC range; (B) This one is measured with 500 KHz laser 50 ns TAC range.

Table 1 List of fluorescence lifetime fitted results of BSA-Au_{25} (lifetime unit: ns)

	A	**B_1**	**T_1**	**B_2**	**T_2**	**B_3**	**T_3**	**B_4**	**T_4**	**χ^2**
First stage fitting results (The fitting result was affected by the range choice)										
2us 1exp	406	1319.2	1.23×10^3							0.98
Second stage fitting results										
50ns 4exp	1085.5	0.001	1.25×10^3	0.01	10.2	0.04	1.97	0.12	0.25	1.12

Considering the fitting result in table 1, it is apparently that there is a micro second range's long lifetime component T_1 when the decay is fitted at TAC range 2 μs. This result is comparable with the result given by Guével [31] and Wu [4]. The first stage fitted result varies from 1.2~1.3μs as fitting range changes. One of them is listed in table 1. The best value to fit the whole decay was tested very carefully and was figured out to be 1.25μs. The short lifetime components were found to be T_2=10.2 ns, T_3=1.97 ns and T_4=0. 25 ns when T_1 was fixed to be 1.25μs.

When the decay curve of reference sample (BSA+NaOH) was fitted, the fitted lifetime values of 3-exponential decay were 0.25 ns, 1.9 ns and 6.8 ns. These fluorescence lifetimes are comparable to those short lifetimes obtained from BSA-Au_{25} samples listed in table 1, implying that the fast fluorescence component in BSA-Au_{25} may mainly arise from BSA.

As BSA is a common plasma protein and when its conformation with pH is changed the BSA-Au_{25} may be sensitive to pH environment. The investigation on the dependence of fluorescence intensity on the pH value, as shown in figure 28, has been described above. Here, the influence of pH on the fluorescence lifetime is investigated. Figure 31 displays the fluorescence decay curves of BSA-Au_{25} at different pH environments. It can be seen that there is no obvious change in the region between pH 9.8 and pH 7.0. Change in decay curve is observed at pH 4.7 and becomes significant as pH further decreases.

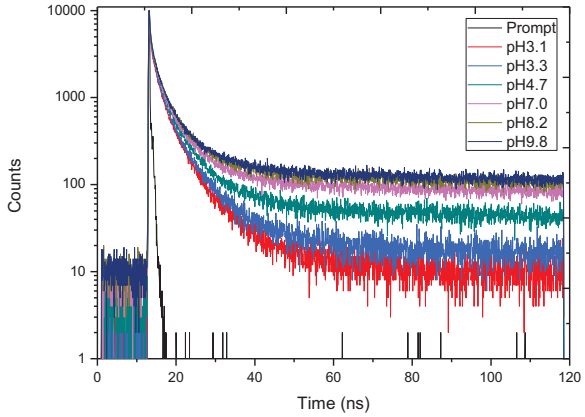

Figure 31 The lifetime of BSA-Au_{25} at different pH

These decay curves were fitted with 4-exponential functions as shown in equation 8. All the fitted constants are listed in table 2. As observed from Figure 31, the shape of the long lifetime component doesn't change apparently when pH value change, so the value of long lifetime component was still assumed to be 1.25 μs and then the possibility of this assumption was justified by considering the value of χ^2. The acceptable goodness of χ^2 in table 2 implies the validity of adopted assumption, also implies that the difference of pH values may not change the instinct lifetime of BSA-Au_{25}. Moreover, it is found that the contribution of a long decay component to the whole decay is falls down when the pH value falls down as shown in figure 32. It implies that the existing BSA-Au_{25} remains its microstructure of fluorescence related parts such as 13 atoms' gold core, 12 atoms' oxidized gold shell and combined sulfur structures. These structures are not been modified when the environmental pH changes. One possible explanation for the decrease of fluorescence is that the amount of fluorophores in the solution is decreased as the pH value reduces. The reduction of fluorophores in the solution is considered to be caused by the fragmentation of gold cores or detachment of gold core from BSA, resulting from the structural modification

of BSA as the environmental pH changes.

Table 2 Fitted results for the lifetime decays of BSA-Au_{25} at different pH value with fixed T1 (lifetime unit: ns)

pH	A	B_1	T_1	B_2	T_2	B_3	T_3	B_4	T_4	χ^2
3.1	-78.90	0.01	1.25×10^3	1.04	0.23	0.37	1.82	0.09	6.24	1.14
3.3	-110.69	0.12	1.25×10^3	7.64	0.23	3.39	1.74	0.85	6.30	1.12
4.7	-165.08	0.02	1.25×10^3	0.92	0.26	0.43	1.78	0.11	6.36	1.04
7.0	-234.75	0.04	1.25×10^3	0.87	0.25	0.42	1.72	0.12	6.25	1.06
8.2	-302.36	0.05	1.25×10^3	0.88	0.28	0.40	1.81	0.13	6.32	1.07
9.8	-363.77	0.45	1.25×10^3	6.87	0.24	3.44	1.76	1.01	6.40	1.06

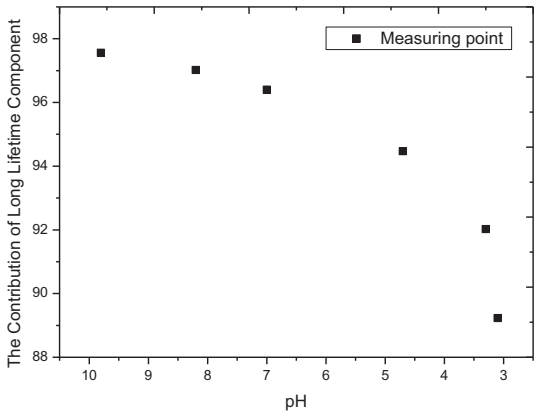

Figure 32 The contribution of long lifetime component to the whole decay.

Furthermore, comparing figure 28 with figure 32, it is apparently that the emission intensity falls down as the contribution of long lifetime component to the whole decay falls down when the pH value falls down. This underlying relationship between these two figures is coincident with the suggestion given in section 3.1.2 and this section that the red emission and the long lifetime component are both correlated with the existence of gold core.

3.1.5 Fluorescence anisotropy of BSA-Au_{25}

The fluorescence anisotropy is calculated following the equation below:

$$r(t) = \frac{I_{VV}(t) - GI_{VH}(t)}{I_{VV}(t) + 2GI_{VH}(t)} \tag{9}$$

Where $I_{VV}(t)$ and $I_{VH}(t)$ are the recorded polarized decay curves where the indexes *VV* and *VH* indicate the orientation of the excitation and emission polarizers respectively. The *G* factor corrects for different transmission efficiencies of polarized light though the detection system and is calculated from the equation below:

$$G = \frac{\int I_{HV}(t)dt}{\int I_{HH}(t)dt} \tag{10}$$

The anisotropy curve can be fitted following the equation below:

$$r(t) = b\exp(-t/\phi) + b_{\infty} \tag{11}$$

Where b is the pre-exponential factor and b_{∞} is an infinity value. Symbol ϕ represents the rotational correlation time. BSA-Au_{25} was assumed to be sphere to simplify the calculation model.

From the Stokes-Einstein relationship, the rotational correlation time ϕ can be calculated out simply following the equation below:

$$\phi = \frac{\eta V}{k_b T} = \frac{4\pi\eta R^3}{3k_b T} \tag{12}$$

Where η, k_b and T indicates the viscosity of the solution, Boltzmann constant and absolute temperature respectively. The volume of the fluorophore is indicated by *V*. Taken together, the radius of the fluorophore can be calculated from the equation

below:

$$R = (\frac{3\phi T k_b}{4\pi\eta})^{1/3} \quad (13)$$

Following those equations above, fluorescence anisotropy related results at different temperature have been calculated out and listed in table 3. The experiment is based on the sample with 0.5mM [Au]. A laser source with wavelength 482nm was adopted in this experiment. LP530 filter was adopted to block the fluorescence from BSA, meanwhile, allow the fluorescence from BSA-Au_{25} to access so that it was affirmative that the fluorescence anisotropy is from BSA-Au_{25}.

Table 3 Fluorescence anisotropy of 20times diluted sample at different temperature

Temp / K	η / mPa s	ϕ / ns	R / nm
277.6	1.54	18.6	4.7
281.4	1.37	19.2	5.0
292.3	1.02	16.1	5.3
297.6	0.90	14.7	5.4
301.0	0.83	15.1	5.6
306.3	0.74	14.8	5.8
311.9	0.66	13.4	5.9

From table 3 the radius of the BSA-Au_{25} cluster is calculated within 4.7~5.9 nm based on a spherical model.

BSA is widely known having a heart shape super-huge single molecule structure [42]. The size of the protein is 3×9×9 nm (thickness×X-axis×Y-axis) in Normal (N) form as shown in Figure 33 [43]. The size of BSA-Au_{25} calculated based on fluorescence anisotropy measurement is comparable but slightly larger than the reported value. It may reflect an increased particle size due to its gold core. The simple

spherical model also introduces error. Nevertheless, this work demonstrated that the size of BSA-Au_{25} can be obtained by fluorescence anisotropy measurement.

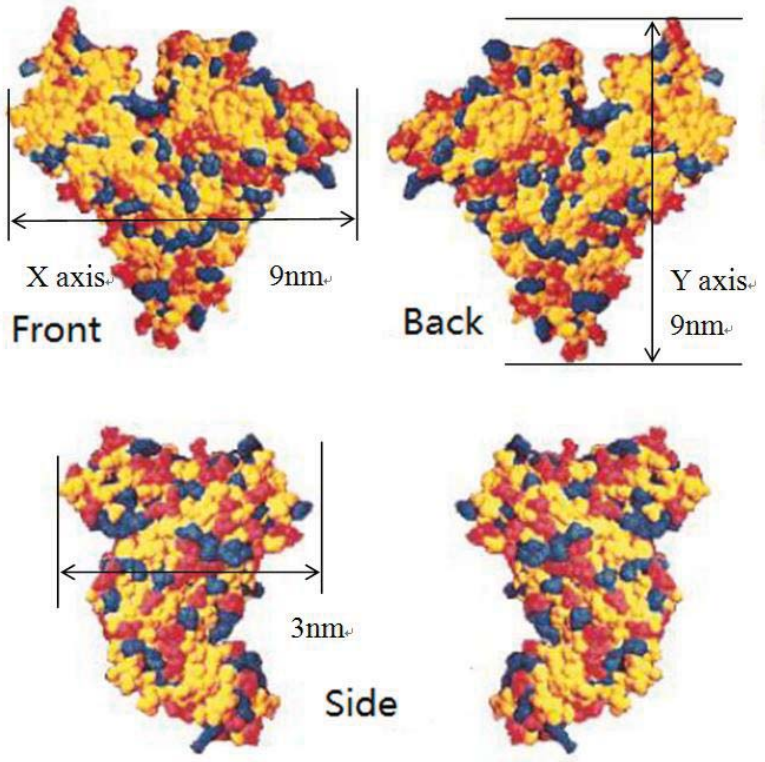

Figure 33 Microstructure of BSA from different view point and its dimensions. Figure is from reference [43]

Figure 34 shows the fluorescence anisotropy decay at different pH value. The fluorescence anisotropy decay changes as pH value changes from 9.8 to 3.3. The further decrease of pH value to 3.1, however, results in an apparent change, as shown with black line in figure 34. The big change in the anisotropy value implies the change of particle size. As shown in table 4, the radius of the clusters increases to around 9.3~11.0 nm, nearly double the size obtained before.

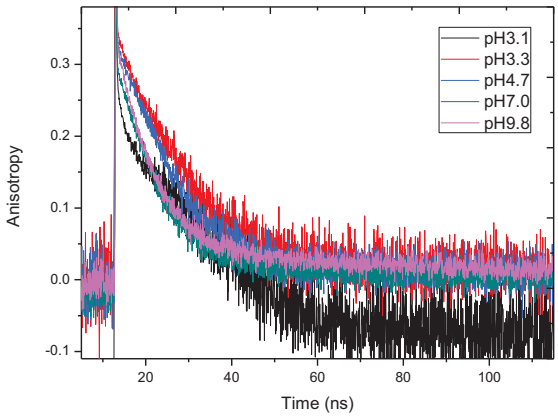

Figure 34 Anisotropy comparison of BSA-Au_{25} at different pH value

Table 4 Fluorescence anisotropy of the sample at pH 3.1

Temp / K	η / mPa s	ϕ / ns	R / nm
283.5	1.3	185.3	11.0
290.3	1.1	98.8	9.5
292.5	1.0	111.2	10.2
296.1	0.9	86.4	9.7
301.6	0.8	65.9	9.3

This result is in line with the conformation change of BSA. It is reported by Carter that there are 3 forms of BSA at different pH value, namely normal (N) form at pH value 8 to 10, fast (F) form at pH 4.3 to 8, and expand (E) form at pH 2.7 to 4.3 [42]. Moreover, recent work carried out by Barbosa in 2010 disclosed that the E form appears at pH<3.5 [44]. It is said in their works that the BSA expand as the pH value decreases, this conclusion is coincident with our work in which the sizes of the BSA coated clusters were doubled as the pH decreased from 9.8 to 3.1. The structural sketches of three forms were as shown in figure 35 [43].

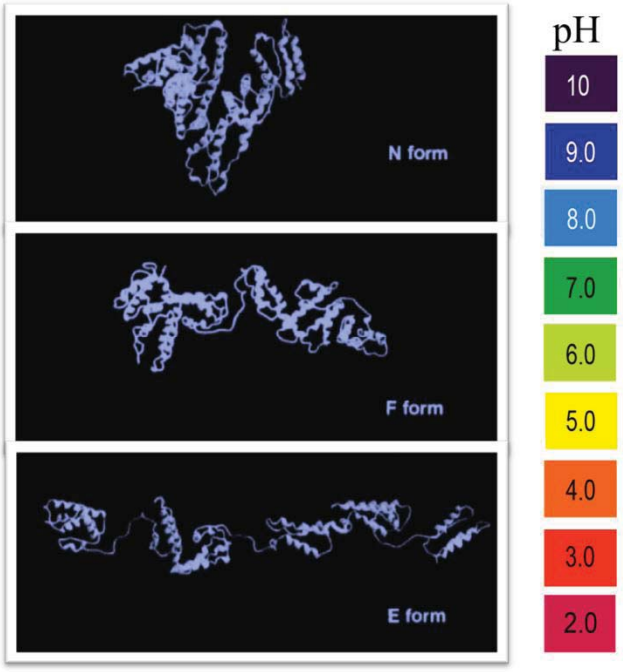

Figure 35 Three types of basic form of BSA at different pH value (Drawn by Carson, 1987)

The size of the BSA in F and E form have been found in Lee's work [45], which are 3 (thickness) ×9 (Y-axis) ×15 (X-axis) nm and 2.5 (thickness) ×10 (Y-axis) ×20~25 (X-axis) nm respectively. The calculated radius of BSA-Au_{25} at pH 3.1 is ~11 nm (22 nm diameter), which is consistent with the reported dimension in E form (20~25 nm). This change in the protein conformation accompanies the significant decrease of fluorescence intensity and change in lifetime as described above, suggesting a dramatic change of cluster structure. More researches are required to support this point.

3.2 Application of BSA-Au_{25} as metal ion sensor

It is reported that AuNCs can be employed in a lot of occasions. One of the typical applications of BSA-Au_{25} is as a bio-sensor to detect metal ions. It is reported that it

can be used to detect mercury ions in the environmental protection field [16, 46]. The fluorescence quenching due to copper ions has also been reported, suggesting a potential of ion sensing in live cells [7, 47]. This work investigated the influence copper ion on the fluorescence of BSA-Au_{25}.

BSA-AuNC is adopted as the sensor to detect copper ions in this project. To extend the experimental result carried out by other researchers, we compared the lifetime difference as well as the intensity difference. The BSA-Au_{25} sample adopted in this experiment is diluted by 100 times from the original prepared sample in which the concentration of [Au] is around 5 mM. The reason why a 100times diluted sample was adopted instead of the former 20times diluted one adopted in previous experiment is that the BSA-Au25 was used as a sensor in this experiment. The lower the concentration, the more sensitive it becomes. Cu^{2+} is offered by adding $CuSO_4$ into the BSA-Au_{25} solution. The fluorescence emission is quenched as shown in figure 36.

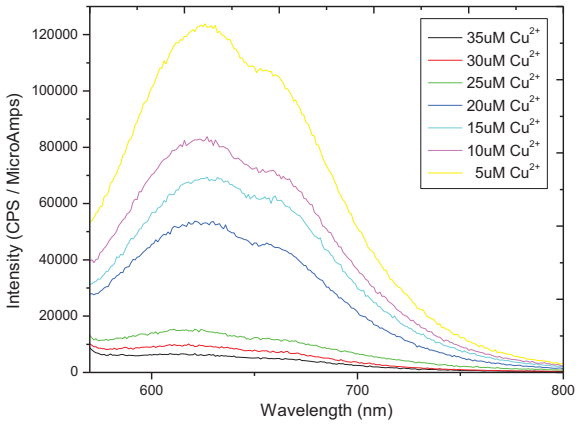

Figure 36 The quenching of the fluorescence emission by adding different quantity of Cu^{2+} ions

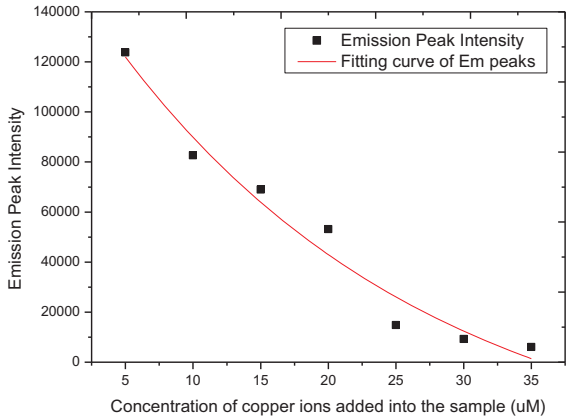

Figure 37 The emission peak intensity against concentration of Cu^{2+} existed in the solution

The emission intensity decreases monotonically as the concentration of [Cu] ions increases, as shown in figure 37. The relationship between emission peak intensity and concentration of copper ions suggests the possibility of quantitative ion sensing. The relationship was represented by equation below:

$$I = 206411e^{\left(\frac{-C}{23.3}\right)} - 44538, \qquad (14)$$

where I represents the intensity, C represents concentration of [Au]. R-Square is 0.95587.

In this project, several different metal ions were added into BSA-Au_{25} samples to see whether there was fluorescence quenching. The test was accomplished by adding Co^{2+} and Zn^{2+} in BSA-Au_{25} solution, shown in figure 38 (a) and (b) respectively. The concentration of [Au] in the BSA-Au_{25} solution is 0.05 mM which is the same as at which the copper ions are tested. From the comparison of figure 36 and figure 38, it is apparently that the BSA-Au_{25} is very sensitive to Cu^{2+} but not so sensitive to Co^{2+} and Zn^{2+} which implies that the BSA-Au_{25} may be a selectivity sensor to Cu^{2+} and Hg^{2+} [16, 46] such harmful ions. Distinction of these two harmful ions may be difficult but it

offers a method to test whether the environment is polluted by one of these two harmful ions. More work needs to be done to test whether BSA-Au_{25} is sensitive to other potential ions such as Fe^{2+}, Fe^{3+}, Ni^{2+} and so on.

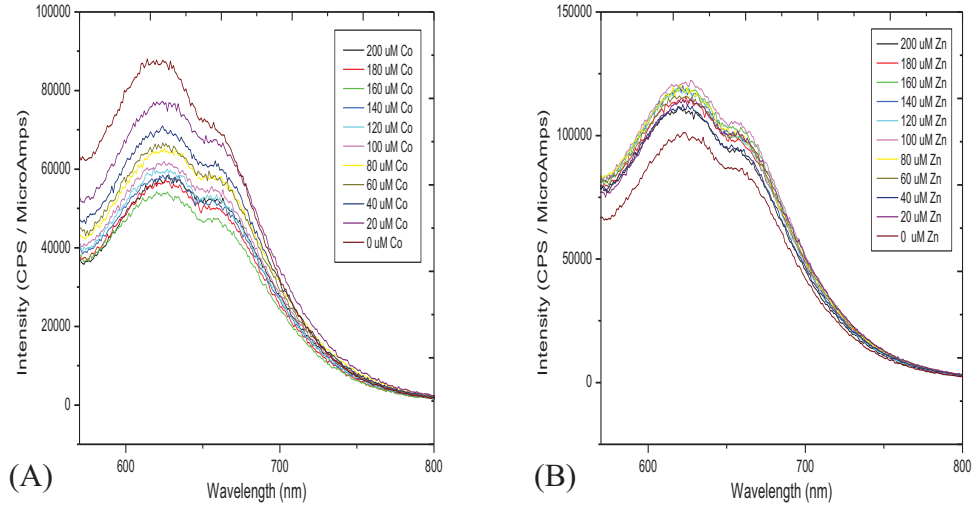

Figure 38 (A) the quenching of fluorescence emission by adding different quantity of Co ions into BSA-Au_{25} solution, (B) the quenching of fluorescence emission by adding different quantity of Zn ions into BSA-Au_{25} solution

To extend the work accomplished by other researchers, different lifetimes of BSA-Au_{25} have been measured to see how the lifetime changes when different quantities of Cu^{2+} ions were added into the solution. The measurement results have been shown in figure 39. Fluorescence lifetimes had been fitted but the χ^2 of the fitting results were extremely high, which means it is impossible to find the numerical model for this lifetime changing procedure with these obtained results. This may be due to the extreme dilution of the BSA-Au_{25} sample. More work need to be done to obtain the precious fitting results to found the numerical model with which the concentration of metal ions can be calculated out with measured lifetime value, even though, the

changing trend of fluorescence lifetime is very apparently as shown in figure 39.

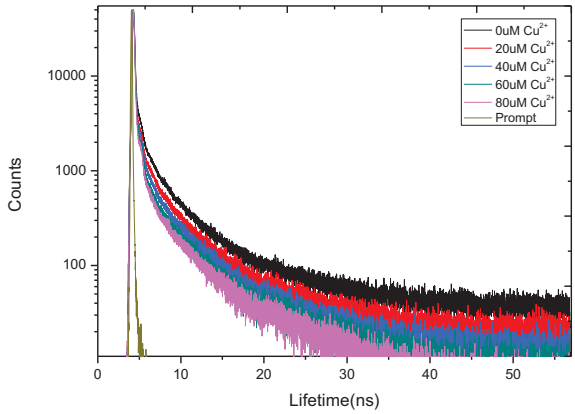

Figure 39 lifetime change by adding different quantity of Cu^{2+} into the BSA-Au_{25} solution

4.Conclusions and Future's Work

Red emit BSA-Au_{25} have been synthesized with a "one step" environmentally friendly wet chemical method. This synthesis method is repeatable. Absorption and emission spectra of the prepared sample have been obtained. It is confirmed that the extreme stable red fluorescence results from gold cores in BSA. The dynamical fluorescence analysis found a long decay lifetime at about 1.2 μs. It is also proved through the fluorescence anisotropy measurement that the cluster size is around 5~6 nm in radius based on a spherical model when the environmental pH is up to 7. When the environmental pH falls down to 3.1 the size of cluster extend to 9~11 nm in radius. Moreover, the prepared BSA-Au_{25} samples were adopted as a Cu^{2+} sensor.

More work need to be carried out to investigate the mechanism of BSA-Au_{25}'s fluorescence. The size selected cluster source can produce gold clusters with good control over size and without coating. Comparing the sample prepared by this method with that synthesized by wet chemical method should help to understand the fluorescence mechanism. Although cluster source is employed to deposit AuNC on the substrate, more improvements need to be done to make the production of large AuNCs possible. For example, using cooling gas introduces gas condensation thus allows to generate large clusters. Two-photon fluorescence technique may also be applied to expand the application of BSA- Au_{25}.

So far, the contribution of gold core and surface bonding in the fluorescence process is still not clear. Other coating may be used to replace the BSA so that the mechanism of fluorescent procedure can be clear after comparing the fluorescent spectrum of coating replaced gold clusters with that of BSA- Au_{25}.

It is worthwhile to investigate the application of BSA-Au_{25} in bio-science because

they are nontoxic, super small, sensitive to metal ions, and have red emission and large stokes shift. The capability of measuring particle size via fluorescence anisotropy, which was demonstrated in this work, suggests a potential of monitoring protein binding and conformation change.

Acknowledgement:

First and foremost, I would like to show my deepest gratitude to my supervisor Dr. Yu Chen, and Prof. David Birch who provided me valuable guidance in every stage of the writing procedure for this thesis. Their unselfish support, enlightening instruction, impressive kindness, patience and rigorous supervision helps a lot on this thesis. Their keen and vigorous academic observation enlightens me not only in this thesis but also in my future study.

I would like to extend my thanks to the academic staff: Jan Karolin, Olaf Rolinski, Jens Sutter, my colleagues: Philip Yip, Mariana Amaro, Yinan Zhang, Jonathan Coulter and Scott Campbell. These kind people taught me so much about the experimental setting skills and fundamental knowledge about nano-physics so that I could solve all the problems I had met. I could feel that this kind support was always around me, which moved me a lot. My sincere appreciation also goes to those kind technicians from the physics Department at the University of Strathclyde: Bob Dawson, Ged Drinkwater, and John Revie. I would not have gotten any results from cluster source without their patient technical support.

Last but not least, I'd like to thank my family, especially my wife Juan, I could not even start this project without their support and encouragement.

Reference:

1. R. Sardar, A.M.F., P. Mulvaney, R. W. Murray, *Gold Nanoparticles: Past, Present, and Future.* Langmuir, 2009. **25**(24): p. 13840-13851.
2. C. J. Lin, C.L., J. Hsieh, H. Wang, *Review- Synthesis of Fluorescent Metallic Nanoclusters Toward Biomedical Application Recent Progress and Present Challenges.* Journal of Medical and Biological Engineering, 2009. **29**(6): p. 276-283.
3. J. Zheng, *Fluorescent Noble Metal Nanoclusters*, in *Chemistry*. 2005, Georgia Institute of Technology.
4. Z. Wu, R.J., *On the Ligand's Role in the Fluorescence of Gold Nanoclusters.* Nano Letters, 2010. **10**(7): p. 2568-2573.
5. J. Zheng, P.R.N., R. M. Dickson, *Highly Fluorescent Noble-Metal Quantum Dots.* Annual Review of Physical Chemistry, 2007. **58**(1): p. 409-431.
6. A. A. Herzing, C.J.K., A. F. Carley, P. Landon, G. J. Hutchings, *Identification of Active Gold Nanoclusters on Iron Oxide Supports for CO Oxidation.* Science, 2008. **321**(5894): p. 1331-1335.
7. C. V. Durgadas, C.P.S., K. Sreenivasan, *Fluorescent Gold Clusters as Nanosensors for Copper Ions in Live Cells.* Analyst, 2011. **136**(933): p. 933-940.
8. C. Huang, Z.Y., K. Lee, H. Chang, *Synthesis of Highly Fluorescent Gold Nanoparticles for Sensing Mercury(II).* Angewandte Chemie, 2007. **119**(36): p. 6948-6952.
9. A. Retnakumari, S.S., D. Menon, P. Ravindran, H. Muhammed, T. Pradeep, S. Nair, M. Koyakutty, *Molecular-receptor-specific, Non-toxic, Near-infrared-emitting Au Cluster-protein Nanoconjugates for Targeted Cancer Imaging.* Nanotechnology, 2010. **21(5)**(055103): p. 1-13.
10. W. Cai, T.G., H. Hong, J. Sun, *Applications of Gold Nanoparticles in Cancer Nanotechnology.* Nanotechnology, Science and Applications, 2008. **1**: p. 17-32.
11. J. Zheng, J.T.P., R. M. Dickson, , *High Quantum Yield Blue Emission From Water-Soluble Au8 Nanodots.* Journal of the American Chemical Society, 2003. **125**(26): p. 7780-7781.
12. J. Zheng, C.Z., R. M. Dickson, *Highly Fluorescent, Water-Soluble,*

Size-Tunable Gold Quantum Dots. Physical Review Letters, 2004. **93-7**(077402): p. 1-4.

13. L. Shang, R.M.D., S. Brandholt, R. Schneider, *Facile Preparation of Water-soluble Fuorescent Gold Nanoclusters for Cellular Imaging Applications.* Nanoscale, 2011. **3**: p. 2009-2014.

14. J. Xie, Y.Z., J. Y. Ying, , *Protein-Directed Synthesis of Highly Fluorescent Gold Nanoclusters.* Journal of the American Chemical Society, 2009. **131**(3): p. 888-889.

15. X. L. Guével, B.H.t., G. Jung, M. Schneider, *NIR-emitting Fuorescent Gold Nanoclusters Doped in Silica Nanoparticles.* Journal of Materials Chemistry, 2010. **21**: p. 2974-2981.

16. H. Wei, Z.W., L. Yang, S. Tian, C. Hou, Y. Lu, *Lysozyme-stabilized Gold Fluorescent Cluster: Synthesis and Application as Hg^{2+} Sensor.* Analyst, 2010. **135**(6): p. 1406-1410.

17. I. Hussain, S.G., Z. Wang, B. Tan, D. C. Sherrington, S. P. Rannard, A. I. Cooper, M. Brust, *Size-Controlled Synthesis of Near-Monodisperse Gold Nanoparticles in the 1−4 nm Range Using Polymeric Stabilizers.* Journal of the American Chemical Society, 2005. **127**(47): p. 16398-16399.

18. Y. Bao, H.Y., C. Zhong, S. A. Ivanov, J. K. Sharma, M. L. Neidig, D. M. Vu, A. P. Shreve, R. B. Dyer, J. H. Werner, J. S. Martinez, *Formation and Stabilization of Fluorescent Gold Nanoclusters Using Small Molecules.* The Journal of Physical Chemistry C, 2010. **114**(38): p. 15879-15882.

19. H. Abe, W.S., B. Tesche, *Optical Properties of Silver Microcrystals Prepared by Means of the Gas Aggregation Technique.* Chemical Physics, 1980. **47**(1): p. 95-104.

20. W. A. de Heer, P.M., *An Improved Laser Vaporization Cluster Source and Time-of-flight Mass Spectrometer.* Zeitschrift für Physik D Atoms, Molecules and Clusters, 1991. **20**(1): p. 437-439.

21. C. Félix, C.S., W. Harbich, J. Buttet, I. Rabin, W. Schulze, G. Ertl, *Ag_8 Fluorescence in Argon.* Physical Review Letters, 2001. **86**(14): p. 2992-2995.

22. S. Fedrigo, W.H., J. Buttet, *Optical Response of Ag[2], Ag[3], Au[2], and Au[3] in Argon Matrices.* 1993. **99**(8): p. 5712-5717.

23. I. Rabin, W.S., G. Ertl, *Light Emission During the Agglomeration of Silver Clusters in Noble Gas Matrices.* Journal of Chemical Physics, 1998. **108**(12): p. 5137-5142.

24. F. Stienkemeier, J.H., W. E. Ernst, G. Scoles, *Laser Spectroscopy of*

Alkali-Doped Helium Clusters. Physical Review Letters, 1995. **74**(18): p. 3592-3595.

25. Grimaud, C., *Deposition and Spectroscopy of Supported Metal Clusters*, in *School of Physics and Astronomy*. 2000, The University of Birmingham.

26. X. Liu, C.L., J. Xu, J. Lv, M. Zhu, Y. Guo, S. Cui, H. Liu, S. Wang, Y. Li, *Surfactant-Free Synthesis and Functionalization of Highly Fluorescent Gold Quantum Dots.* The Journal of Physical Chemistry C, 2008. **112**(29): p. 10778-10783.

27. R. L. Whetten, R.C.P., *Nano-Golden Order.* Science, 2007. **318**(5849): p. 407-408.

28. P. D. Jadzinsky, G.C., C. J. Ackerson, D. A. Bushnell, R. D. Kornberg, *Structure of a Thiol Monolayer-Protected Gold Nanoparticle at 1.1 Å Resolution.* Science, 2007. **318**(5849): p. 430-433.

29. M. W. Heaven, A.D., P. S. White, K. M. Holt, R. W. Murray, *Crystal Structure of the Gold Nanoparticle* $[N(C_8H_{17})_4][Au_{25}(SCH_2CH_2Ph)_{18}]$. Journal of the American Chemical Society, 2008. **130**(12): p. 3754-3755.

30. G. A. Simms, J.D.P., P. Zhang, *Structural and Electronic Properties of Proteinthiolate-protected Gold Nanocluster With "Staple" Motif A XAS, L-DOS, and XPS Study.* The Journal of Chemical Physics, 2009. **131**(214703): p. 1-9.

31. X. L. Guével, B.H.t., G. Jung, K. Hollemeyer, V. Trouillet, M. Schneider, *Formation of Fluorescent Metal (Au, Ag) Nanoclusters Capped in Bovine Serum Albumin Followed by Fluorescence and Spectroscopy.* The Journal of Physical Chemistry C, 2011. **115**(22): p. 10955-10963.

32. S. Rath, S.N., D. Palagin, V. Matulis, O. Ivashkevich, S. Maki, *Aqueous-based Synthesis of Atomic Gold Clusters: Geometry and Optical Properties.* Applied Physics Letters, 2010. **97**(053103): p. 1-3.

33. S. Link, A.B., S. FitzGerald, M. A. El-Sayed, T. G. Schaaff, R. L. Whetten, *Visible to Infrared Luminescence From a 28-Atom Gold Cluster.* The Journal of Physical Chemistry B, 2002. **106**(13): p. 3410-3415.

34. F. Parmigiani, G.S., G. P. Ferraris, *Optical Properties of Sputtered Gold Clusters.* Journal of Applied Physics, 1985. **57**(7): p. 2524-2528.

35. A. Nijamudheen, A.D., *Odd-Even Oscillations in Structural and Optical Properties of Gold Clusters.* Journal of Molecular Structure: THEOCHEM, 2010. **945**: p. 93-96.

36. H. Duan, S.N., *Etching Colloidal Gold Nanocrystals With Hyperbranched and*

Multivalent Polymers: A New Route to Fluorescent and Water-Soluble Atomic Clusters. Journal of the American Chemical Society, 2007. **129**(9): p. 2412-2413.

37. N. Schaeffer, B.T., C. Dickinson, M. J. Rosseinsky, A. Laromaine, D. W. McComb, M. M. Stevens, Y. Wang, L. Petit, C. Barentin, D. G. Spiller, A. I. Cooper, R. Lévy, *Fluorescent or Not? Size-dependent Fluorescence Switching for Polymer-stabilized Gold Clusters in the 1.1-1.7 nm Size Range.* Chemical Communications, 2008(34): p. 3986-3988.

38. C. J. Lin, T.Y., C. Lee, S. H. Huang, R. A. Sperling, M. Zanella, J. K. Li, J. Shen, H. Wang, H. Yeh, W. J. Parak, W. H. Chang, *Synthesis, Characterization, and Bioconjugation of Fluorescent Gold Nanoclusters Toward Biological Labeling Applications.* ACS Nano, 2009. **3**(2): p. 395-401.

39. D. Lim, C.H., G. Ganteför, Y. D. Kim, *Model Catalysts of Supported Au Nanoparticles and Mass-selected Clusters.* Physical Chemistry Chemical Physics, 2010. **12**(46): p. 15172-15180.

40. R. Hill, P.W.M.B., *The Development of C_{60} and Gold Cluster Ion Guns for Static SIMS Analysis.* Applied Surface Science, 2004. **231-232**: p. 936-939.

41. Lakowicz, J.R., *Principles of Fluorescence Spectroscopy*. 3 ed. 2006: Kluwer Academic/Plenum Publishers.

42. D. C. Carter, J.X.H., *Structure of Serum Albumin*, in *Advances in Protein Chemistry*, J.T.E.F.M.R. C.B. Anfinsen and S.E. David, Editors. 1994, Academic Press. p. 153-203.

43. D. Ievlev, I.R., W. Schulze, G. Ertl, *Light Emission in The Agglomeration of Silver Clusters.* Chemical Physics Letters, 2000. **328**(1–2): p. 142-146.

44. L. R. S. Barbosa, M.G.O., F. Spinozzi, P. Mariani, S. Bernstorff, R. Itri, *The Importance of Protein-Protein Interactions on the pH-Induced Conformational Changes of Bovine Serum Albumin: A Small-Angle X-Ray Scattering Study.* Biophysical journal, 2010. **98**(1): p. 147-157.

45. Lee, C.T., K.A. Smith, and T.A. Hatton, *Photocontrol of Protein Folding: The Interaction of Photosensitive Surfactants with Bovine Serum Albumin†.* Biochemistry, 2004. **44**(2): p. 524-536.

46. D. Hu, Z.S., P. Gong, P. Zhang, L. Cai, *Highly Selective Fluorescent Sensors for Hg^{2+} Based on Bovine Serum Albumin-capped Gold Nanoclusters.* Analyst, 2010. **135**(6): p. 1411-1416.

47. H. Liu, X.Z., X. Wu, L. Jiang, C. Burd, J. Zhu, *Rapid Sonochemical Synthesis Of highly Luminescent Non-toxic AuNCs and Au@AgNCs and Cu (ii) Sensing.*

Chemical Communications, 2011. **47**(14): p. 4237-4239.

48. Alton, G.D., *An Axial Geometry Cesium Sputter Negative Ion Source With Continuous Tungsten Surface Ionizer.* Nuclear Instruments and Methods in Physics Research Section A: Accelerators, Spectrometers, Detectors and Associated Equipment, 1986. **244**(1-2): p. 133-141.

49. S. G. Hall, M.B.N., A. W. Robinson, R. E. Palmer, *Compact Sputter Source for Deposition of Small Size-selected Clusters.* Review of Scientific Instruments, 1997. **68**(9): p. 3335-3339.

50. Leeds, S.M., *Characterisation of the Gas-Phase Environment in a Microwave Plasma Enhanced Diamond Chemical Vapour Deposition Reactor using Molecular Beam Mass Spectrometry*, in *Department of Physical Chemistry*. 1999, University of Bristol.

Appendix 1 List of Abbreviation

NC(s): nano-cluster(s)

BSA: bovine serum albumin

AuNP(s): gold nano-particle(s)

AuNC(s): gold nano-cluster(s)

PAMAM: poly(amido) amine dendrimer

THPC: Tetrakis Hydroxymethyl Phosphonium Chloride

DNA: Deoxyribonucleic acid

HTMP: high temperature matrix preparation techniques

XPS: X-ray photoelectron spectroscopy

TA: thioctic acid

TPP: triphenyl phosphine

TCB: thiocholine bromide

MUA: 1-mercaptoundecanoic acid

PVP: polyvinylpyrrolidone

DT: 1-dodecanethiol

DA: dodecylamine

TCSPC: Time-correlated single-photon counting

O.D: optical density

CFD: constant fraction discriminators

TAC: time to amplitude converter

PGA: programmable gain amplifier

ADC: analog-to-digital converter

Appendix 2 Production of AuNCs in Physical Method

A 2.1 Physical method through cluster source

Different from the chemical method, the physical way can more accurately produce gold cluster in target size. G. Alton developed a cesium based sputter source which can produce size-selected clusters[48], based on model of “Cluster Source” developed by Hall [49]. The equipment is shown in Figure 40. Part I is the diffusion pump which is used to keep the sputtering/ion optics chambers under high vacuum; while Part II is a turbo molecule pump which is used to keep the wien filter/sample holder working in a high vacuum environment. Normally, the system works when the pressure is around 10^{-7}torr.

Firstly the vaporized Cs entered into the chamber, and was ionized on the surface of ionizer. Sputtering process occurred subsequently on the surface of target sample. Negative charged gold ions went through the ions focusing chamber and then condensed into a beam. Passing through a Wien filter, the selected ions accessed the 10°-deflection hall and landed on the surface of sample holder finally.

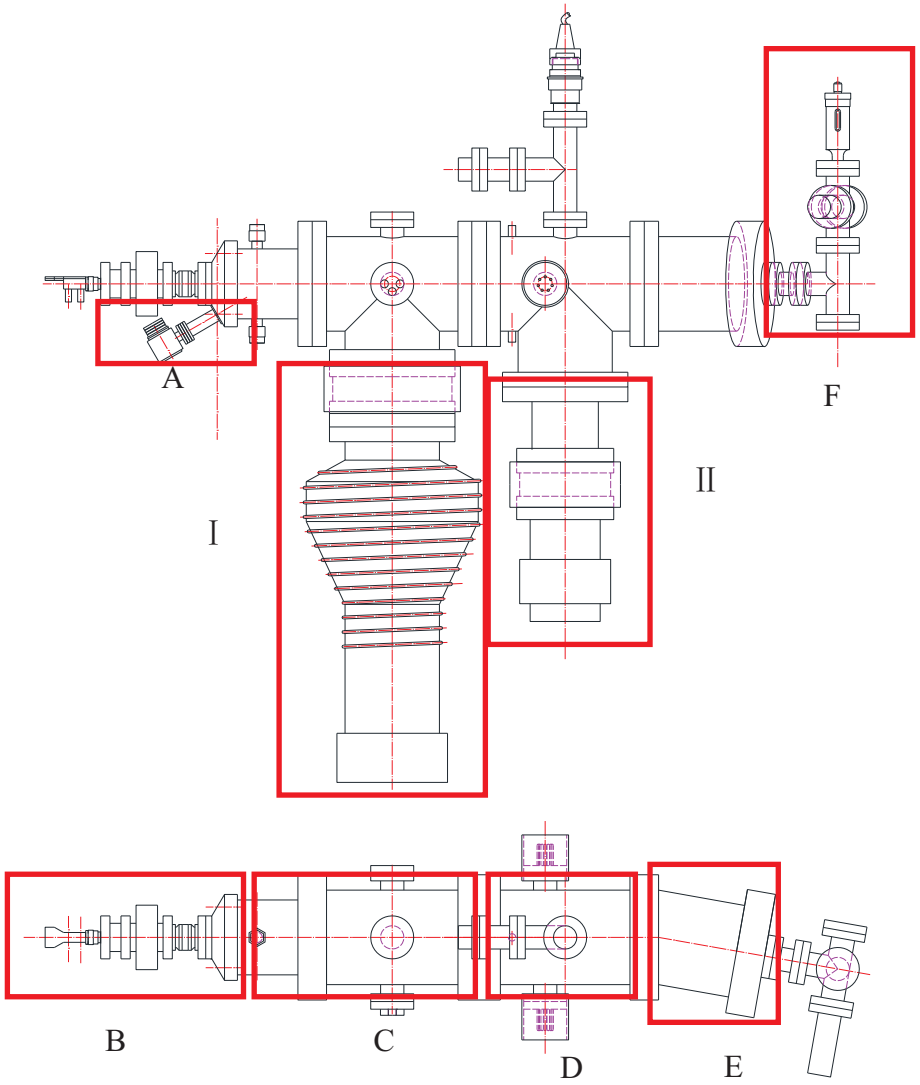

Figure 40 Sketch of cluster source: A, cesium oven which works based on the thermodynamic equilibrium surface ionization phenomenon; B, target holder/sputtering chamber; C, ion optic chamber, two levels lens inside used to focus the beam; D, Wien filter chamber in which mass selection occurred; E, 10°-deflection hall.

A 2.1.1 Ionization/Sputtering process

The cesium oven works based on the thermodynamic equilibrium surface ionization phenomenon. It can be described by the formula below:

$$Cs + Energy \rightarrow Cs^{+} + e^{-} \tag{15}$$

Ionization energy of cesium is only 382KJ/mol, which is the lowest one among the materials. In our cluster source, ionization process occurs on the surface of the tungsten ionizer. As the surface temperature of the ionizer is up to 1100℃, the cesium atoms are ionized, then hit on the target sample under 1.5~1.8kV high voltage. Details about the ionization section can be seen in Figure 41.

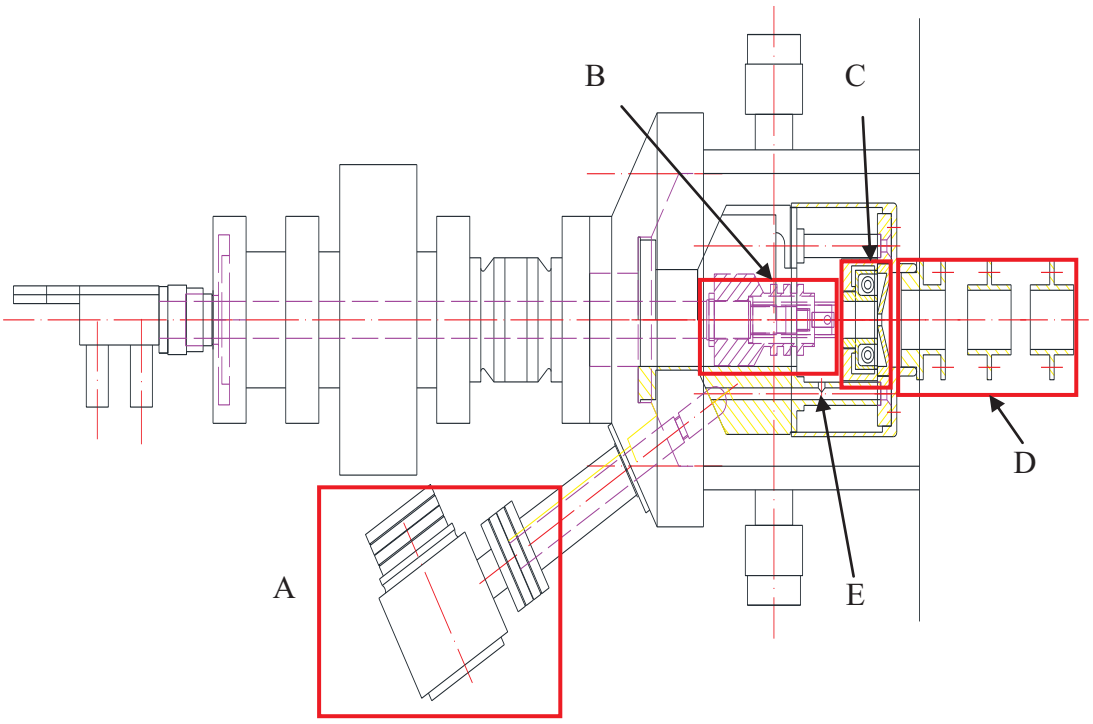

Figure 41 Scheme of the ionization/sputtering chamber, A, cesium oven; B, target holder and bulk gold target sample; C is ionizer with Mo filament and W shell, D is first lens, E is gas hole through which Cs vapor goes into the chamber

Sputtering process is shown in Figure 42. During the process of the incident ions hitting the surface of target metal, the energy is transferred from primary ion to target atom. If the energy is high enough, the atom takes off from the surface of target sample, which achieves the sputtering process.

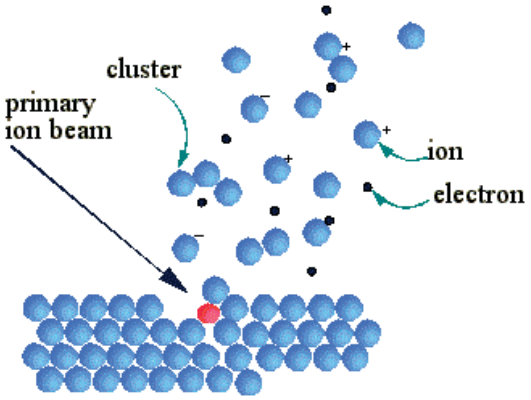

Figure 42 The scheme of sputtering process. Red dot represents incident ion (Cs^+); blue dots represent target atoms/ions; black dots represent electrons [50].

In our experiment, Cs^+ ions are the primary ions. When they hit on the surface of gold bulk, the $Au_{(n)}^-$ ions are sputtered. The number *n* may vary from one to several dozens.

A 2.1.2 Mass selection

Wien filter is adopted to achieve the mass selection. A Wien filter as shown in Figure 43 is a device consisting of perpendicular electric and magnetic fields. The principle of it is shown in Figure 44.

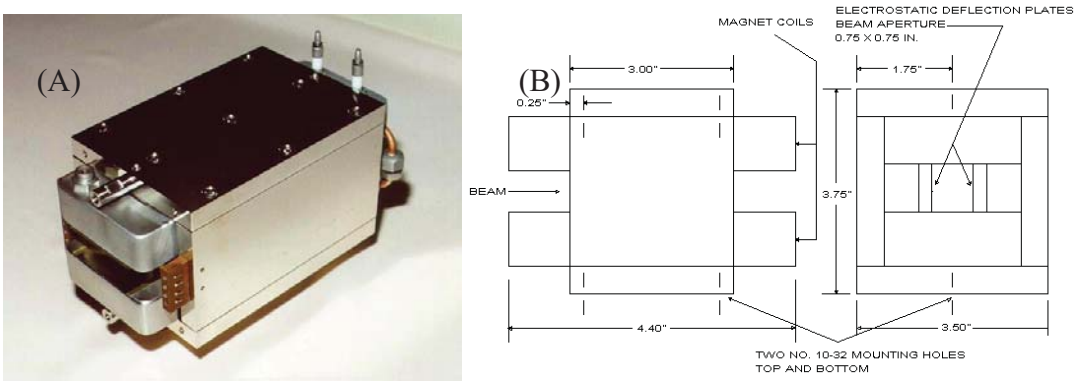

Figure 43 (A) The photograph of a Wien filter. (B) The sketch of a Wien filter. Figures are from homepage of Colutron Research Corporation (http://www.colutron.com/products/kit/kit.html)

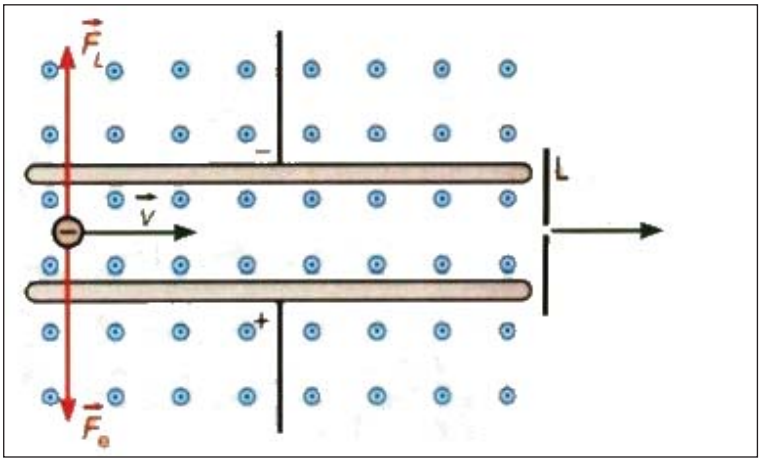

Figure 44 The fundamental principle to illustrate the mechanism of Wien filter. The flying charged clusters forced by perpendicular electric and magnetic fields. Only the clusters with an equilibrium force will pass through the aperture.

The clusters with velocity shown in equation below can access the filter without deflection, while others flying away

$$v_0 = \frac{E}{B} \tag{16}$$

A 2.1.3 Deposition on the substrate

The deposition process occurs in a few different ways as shown in Figure 45. Soft landing means that cluster deposits on the surface of substrate relatively slowly herein can hold its structure. In this deposition method, velocity of cluster should be controlled. The substrate must be soft enough to hold the cluster gently, meanwhile, toughness is needed for the substrate so that it can hold the cluster on its surface but not allow the cluster embedding inside it. Only if the cluster is soft landed on the surface of substrate can the optical property inspection be carried out. The reflection means the cluster will be reflected back off the surface of substrate, in this situation, nothing can be found on the substrate. The plastic deformation means that the microstructure of cluster changes when the cluster lands on the substrate, then, subsequent property inspection means nothing. Fragmentation, partial implantation, sputtering and damage make the microstructure of cluster changes as well, so they all affect the subsequent inspections. In embedding method, cluster was embedded under the surface of substrate, which makes subsequent optical inspection impossible.

In our project, soft substrate is prepared for soft landing. In the future, a bias voltage may be placed in front of our substrate to slow down the landing clusters so that soft landing clusters can be achieved.

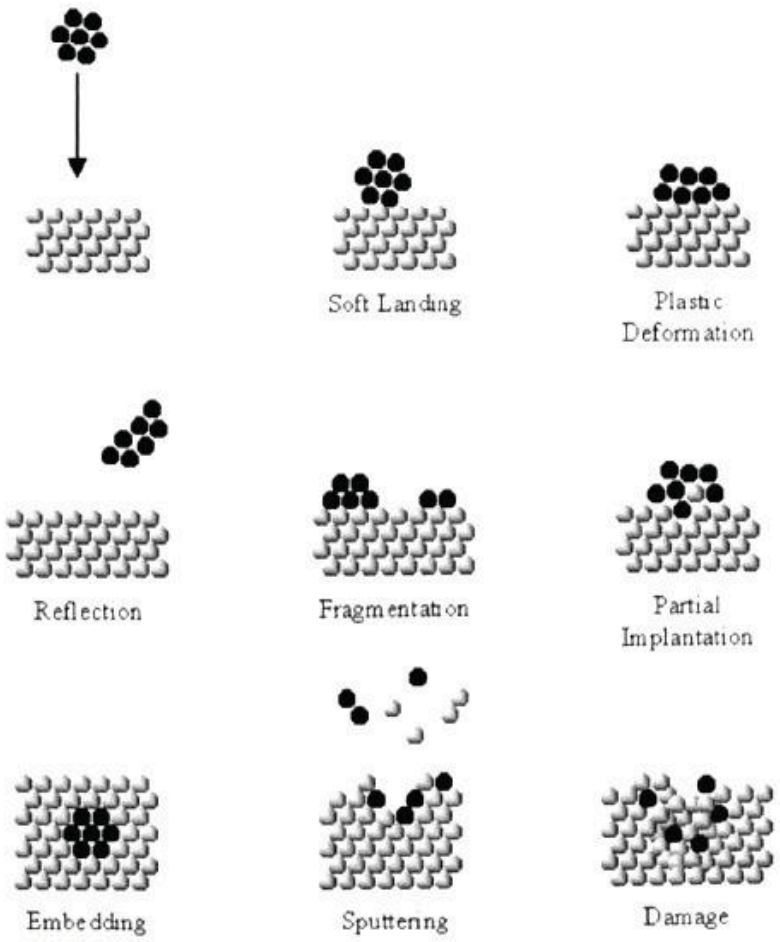

Figure 45 Schematic graph of different landing process. Soft landing and embedding process was expected in this project. The figure is derived from reference [25]

A 2.2 Generation of size selected AuNCs

To facilitate a size dependent fluorescence study, effort has been made to explore the experimental condition to generate NCs of designed sizes. In the experiment, cluster beam current against magnetic field voltage has been obtained. Then it can be transfered to a mass spectrum based on the equation 17

$$M = 2qV(B/E)^2 \tag{17}$$

In equation 17, M represents mass of a cluster, q represents the charge of a cluster, V represents accelerate voltage, B is the strength of magnetic field in Wien filter, and E is the electrical field in Wien filter.

The mass spectrum thus obtained is shown in Figure 46.

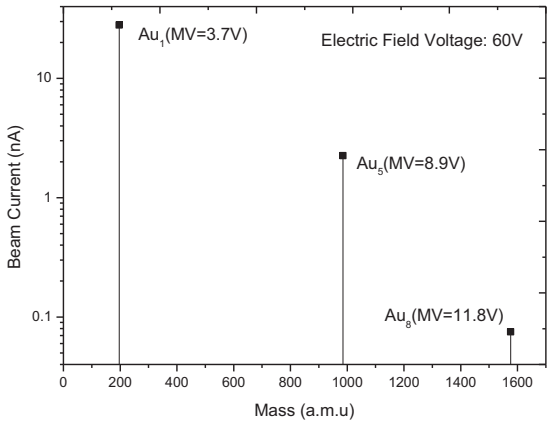

Figure 46 Mass spectrum of our cluster source

From the spectrum above, three types of clusters have been obtained. The first point represents single atom, the second one represents Au_5 cluster while the last one represents Au_8 cluster. The beam current of bigger cluster is beyond the detection limit in this setup.

Bare Au_{25} is possible to be produced by add cooling system on the equipment to aggregate separated clusters on their way to the sample holding after they were sputtered. Once bare Au_{25} clusters are obtained, the investigation of its optical properties may give the direct evidence to explain many optical phenomena such as the existence of the long lifetime component.